Professur für Hydrologie
der Albert-Ludwigs Universität Freiburg i. Br.

Lina Stein

Application of a New Formulation for Hydrologic Transport Using Time-Variable Transit Time Distributions

Masterarbeit unter Leitung von Dr. Andreas Hartman
Freiburg i. Br., September 2016

Professur für Hydrologie
der Albert-Ludwigs Universität Freiburg i. Br.

Lina Stein

Application of a New Formulation for Hydrologic Transport Using Time-Variable Transit Time Distributions

Referent: Dr. Andreas Hartmann
Korreferent: apl. Prof. Dr. Jens Lange

Masterarbeit unter Leitung von Dr. Andreas Hartman
Freiburg i. Br., September 2016

Acknowledgements

This work would not have been possible without the support and encouragement of quite a few people. First, I would like to thank my supervisor Dr. Andreas Hartmann for his continued help and advice throughout the whole master thesis phase. Offering time and guidance as well as unlimited optimism proved a great help both in regard to the thesis and my academic future. My special appreciation goes to Prof. Ciaran Harman, Johns Hopkins University. Without his patient explanations of complex formulas, theories and concepts whenever I was baffled, this work would never have been completed. I would further like to thank Dano Wilusz, Ph.D. student at Johns Hopkins University, and the Landscape Hydrology group for their warm welcome in Baltimore and their advice and assistance throughout my stay. My gratitude goes to Benedikt Heudorfer who offered guidance and help with my first steps through rSAS. I would like to thank apl. Prof. Jens Lange and the Chair of Hydrology for their comments and advice after the presentation of my thesis. I would like to give my sincere thanks to the Verband der Freund der Universität Freiburg and Förderverein Hydrologie for their financial support of my research visit to Johns Hopkins University. I am very grateful for the continued assistance from my family and friends.

Abstract

Karst systems are a common geologic feature throughout the world and are often used as drinking water sources for the local population. The aquifers are however, due to their specific properties, at risk of contamination and changes through global warming. To meet these challenges a thorough understanding of karst properties and solute transport is necessary. The new age-ranked StorAge Selection (rSAS) framework might offer a widely applicable solution to model solute transport in a catchment, but has not been tested in a variable flow environment such as karst. A minor hypothesis that was discussed answered the question, if rSAS could be regarded as a grey-box model, which offers additional information on top of solute transport, or a black box model. To test the new framework it was applied in a well investigated karst catchment in southern Spain. The predicted output concentration for two solutes, SO_4^{2-} and Cl^-, displayed high concordance with the observed concentration in the spring discharge. A Kling-Gupta-Efficiency of 0.8 was reached for SO_4^{2-} and 0.71 for Cl^-, which surpassed the benchmark model VarKarst. The hypothesis that rSAS is suitable to model karst solute transport can be accepted. As further information about the aquifer can be drawn from the rSAS results, it is concluded that rSAS is a grey box model.

Keywords: rSAS, karst, transit time, StorAge Selection function (SAS), enrichment function, time-variant

Zusammenfassung

Karst ist eine geologische Geländeform, die global weiterverteilt vorkommt. Aquifere in Karstgebieten versorgen weltweit einen signifikanten Teil der Bevölkerung mit Trinkwasser, sind jedoch anfällig für Kontamination und Veränderungen durch den Klimawandel. Um diesen Herausforderungen zu begegenen ist ein gründliches Verständnis der Eigenschaften und des Stofftransportes im Aquifer unablässig. Eine neue Methode zur Vorhersage von Stofftransport, age-ranked StorAge Selection (rSAS), ist möglicherweise vielseitig einsetzbar und wäre damit auch in Karstgebieten mit einer hohen zeitlichen und räumlichen Variabilität des Fließverhaltens eine Alternative zu bisherigen Ansätzen. Weiterhin wird diskutiert, ob dieser Ansatz als Greybox-Modell, das mehr als nur Stoffkonzentrationen modellieren kann oder als Blackbox-Modell aufgefasst werden kann. Um beide Hypthesen zu beantworten, wird rSAS in einem bereits gut untersuchtem Gebiet in Südspanien angewendet. Die modellierten Konzentrationen für die beiden Stoffe $SO_4{}^{2-}$ und Cl^- zeigen, dass eine hohe Übereinstimmung mit den beobachteten Konzentrationen im Abfluss erreicht werden konnte. Für $SO_4{}^{2-}$ wurde ein Kling-Gupta-Efficiency-Wert von 0.8 erzielt und Cl^- erreichte eine KGE-Wert von 0.71, sodass das Vergleichsmodell VarKarst übertroffen wurde. Die Hypothese, dass rSAS dafür geeignent ist Stofftransport in Karst zu modellieren, konnte bestätigt werden. Da das Modell auch weitere Schlussfolgerungen zum Fließverhalten im Aquifer zulässt, kann es als ein Greybox-Modell angesehen werden.

Stichworte: rSAS, Karst, Verweilzeit, StorAge Selection function (SAS), Lösungsfunktion, instationär

Contents

List of Figures

List of Tables

1 Introduction

1.1 Introduction

Karstic rocks are widely distributed and can be found all across the ice-free land masses of the globe, as portrayed by the global karst map in Figure 1.1. It is estimated that 20 - 25 % of the global population rely in parts or entirely on drinking water resources from these regions, which make karst aquifers in addition to alluvial aquifers one of the most crucial aquifer formations of the world (Bakalowicz, 2005; Ford and Williams, 2007). Carbonate rocks cover 35 % of the surface area of Europe and in some European countries up to 50 % of the total drinking water demands are met by karst groundwater. In a few areas it is the only available freshwater sources for the local population and an invaluable part of the drinking water supply (Andreo et al., 2008; COST 65, 1995; Zwahlen, 2004). Especially in Mediterranean regions, where the research catchment of this study is located, freshwater supply from karst still has room for development and could help to meet increasing demands (Andreo et al., 2008). However, a prerequisite for the usage of karst catchments as drinking water sources is a thorough analysis of the amount of water resources available, the quality of freshwater, sustainable management options and potential risks (Ford and Williams, 2007). Karst aquifers are, more than other aquifers, subject to two risks which impact freshwater supply and require careful management: climate change and contamination. Karst systems have highly complex flow regimes, where changes in the environmental parameters can impact groundwater flow (Bakalowicz, 2005). The predicted impact of climate change on the Mediterranean area are higher temperatures and less precipitation (Christensen et al., 2007). The ensuing droughts can especially affect recharge rates and decrease available drinking water amounts in the long term (Hartmann, Mudarra, et al., 2014; Milly et al., 2005). Karst aquifers are furthermore at risk of possible contamination. The duality of karst systems leads to a dual vulnerability to contaminants that are transported both very quickly and

very slowly. The quick transport through the conduit system impedes usual processes of contaminant decrease such as adsorption, degradation and filtration. This way contaminated water might reach drinking water wells more quickly preventing the application of mitigation measures. At the same time the contaminant might potentially be stored and released slowly from the karst matrix, which means the corresponding well is lost for drinking water production for a longer period of time (Butscher and Huggenberger, 2009; Harman, 2015; Zwahlen, 2004). A working model of the flow system is thus an invaluable step in the protection and conservation of aquifers against contamination. A model that can predict travel times for solutes found naturally in the system will be able to provide information about contaminant transport and the period of pollution (Ghasemizadeh et al., 2012; Kirchner et al., 2000). To ensure safe current and future drinking water supply from karst aquifers a close study of system characteristics is essential. The new framework tested on a karst catchment in this study was developed by Harman, (2015) and might offer an improved way to model solute transport and determine transit times.

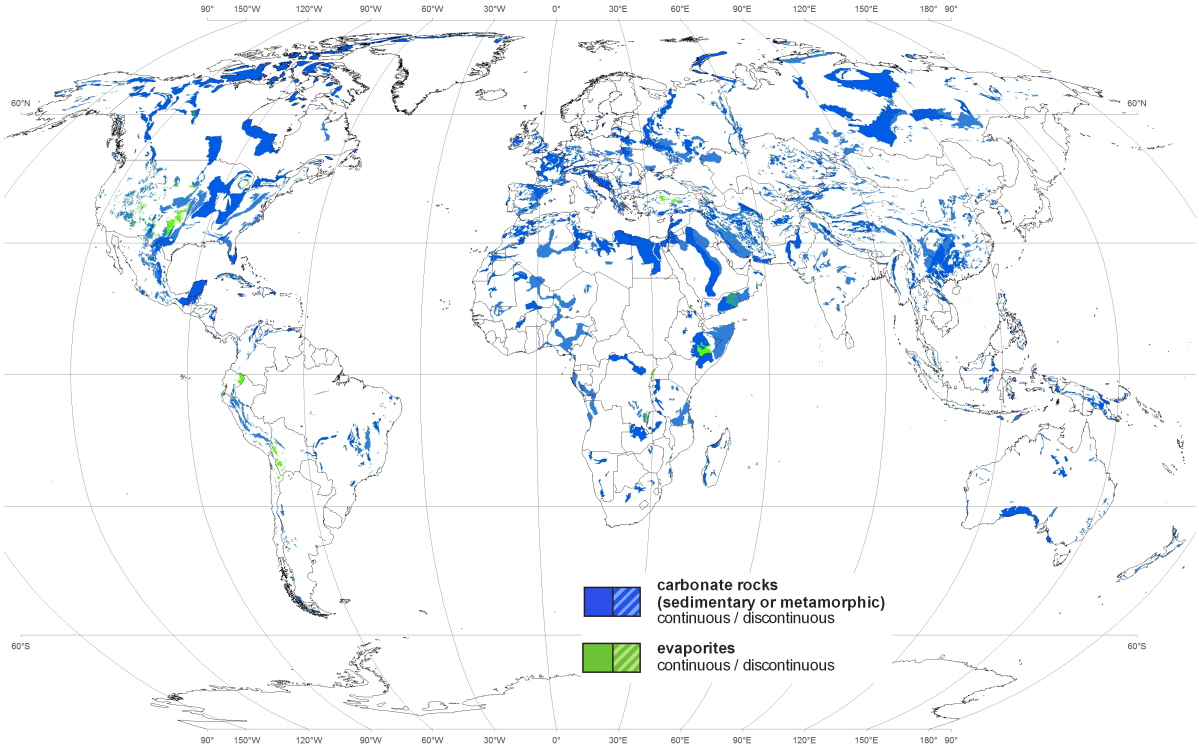

Figure 1.1: Map of the world displaying carbonate and evaporite deposits, which indicate potential karst landscapes (Stevanović et al., 2016)

1.2 State of knowledge

1.2.1 Assessment of karst water resources

Karst characteristics

Karst is a type of landscape, which is formed by the dissolution of carbonated rock such as limestone, dolostone or dolomite rock, through the contact of CO_2 and precipitation. CO_2 generates in contact with water carbonic acid, which reacts with the carbonate rocks, as Equation 1.1 illustrates. It is a continous process which forms typical karst landscapes.

$$CaCO_3 + CO_2 + H_2O \rightleftharpoons Ca^{2+} + 2\,HCO_3^- \tag{1.1}$$

If water accumulates at depressions in the relief and infiltrates through fissures and preferential flow paths, they are subject to more dissolution than the surrounding areas and form characteristic surface pattern above ground such as dolines, swallow holes, karren, dry valleys and poljes (Hartmann, Goldscheider, et al., 2014). The weathered surface of the carbonate rock is called "epikarst". Figure 1.2 depicts, how the water percolates through the epikarst downwards into the saturated zone, although it can sometimes function as a storage as well (Williams, 2008). The dissolution of preferential flow paths underground leads to the creation of fractures, karst conduits and caves. As a result karst aquifers have a high spatial heterogeneity on the surface and subsurface resulting in an equally varying water distribution throughout the aquifer (Goldscheider and Drew, 2007). It additionally adds a variability to infiltration, recharge, flow and storage, which is often described as the duality of karst aquifers in four aspects:

1. A karst aquifer is either recharged locally (autogenic) or the water flows into the aquifer from adjoining non-karst areas (allogenic) as illustrated by Figure 1.2.
2. Infiltration either occurs quickly through sinkholes or dolines or slowly through soil, epikarst and karst matrix.
3. Subsurface water flow is respectively quick in conduits or caves and slow through pores and sometimes fissures.
4. Water storage is small in the conduit system, although it can transport significant amounts of water in a short time period, and large in the karst matrix, where up to 99 % of the water is stored.

These dualities lead to a high temporal variability of the discharge with a fast response to precipitation events, which can increase flow several orders of magnitude (Ford and Williams, 2007; Ghasemizadeh et al., 2012; Goldscheider and Drew, 2007; Maloszewski et al., 2002; Sauter et al., 2006).

Assessment of Karst water resources

The duality of karst aquifers makes the assessment of karst water resources a challenging task. The common way is to combine several methods to analyse the flow system as accurately as possible in regard to discharge reaction, storage and contaminant flow. A first step in water resource exploration are speleological investigations, where the cave

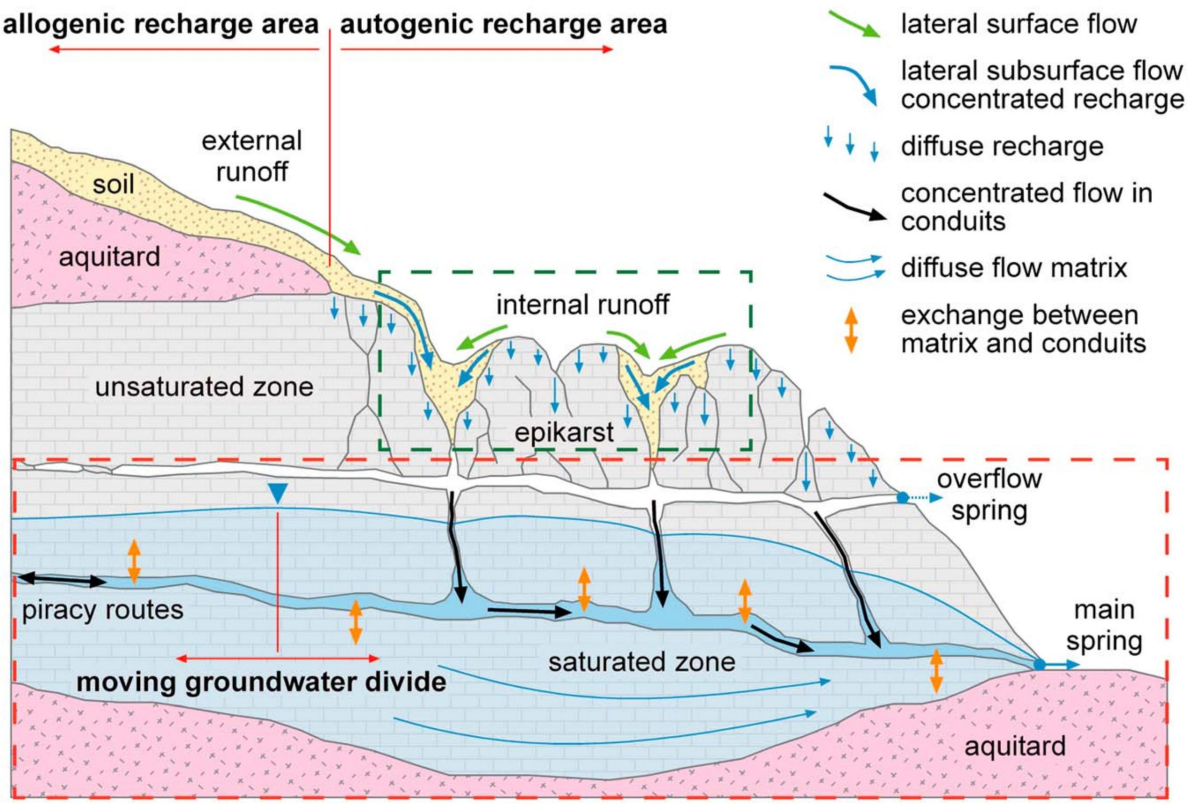

Figure 1.2: Diagram of a conceptual karst aquifer, which includes processes and landscape features distinctive in karst areas. The green dashed line marks the epikarst, the red dashed line the groundwater processes (Hartmann, Goldscheider, et al., 2014)

system is examined, which is exclusive for karst catchments and can give an overview over the conduit network and potential starting points for further inquiries. However, as the conduit system makes up only a small part of the catchment, it does not provide conclusive information for a thorough analysis. These kind of investigations are furthermore only possible in karst systems with accessible caves (Ford and Williams, 2007; Goldscheider and Drew, 2007). Bakalowicz, (2005) suggests to approach the assessment of a karst catchment by first determining the internal structure of the aquifer through geophysical methods. Seismic measurements can supply information about the geological structure such as rock strata, possible fractures or layer density. Measuring minor changes in the earth's gravity are then used to locate potential sinkholes, inaccessible

caves or conduits as well as estimate porosity. Electromagnetic methods can also be used to locate conduits, though scope of application and results vary with different methods (Debeglia et al., 2006; Goldscheider and Drew, 2007). The obtained knowledge supports the next step which is to outline the catchment (Bakalowicz, 2005; Ford and Williams, 2007; Goldscheider and Drew, 2007). For a non-carbonate area the borders of the catchment are assumed to correspond with the surface topography in form of mountains or ridge which define a clear watershed. In karstic areas the subsurface structure can lead to a catchment much smaller or larger than the surface suggests. Suitable methods to determine the catchment area are therefore geomorphological mapping or tracer application (Bakalowicz, 2005). Geomorphological mapping utilises the distinct landscapes that are typcial for karst regions to find points of recharge such as swallow holes or dolines as well as points of discharge such as springs. Dolines and surface forms like karren are an indicator for the spatial orientation of possible fracturing and can hint the direction of the conduit system (Goldscheider and Drew, 2007).

Application of natural and artificial tracer

Another method to analyse karst water resources, catchment limits and recharge area is the application of natural and artificial tracers. Artificial tracers are easily detectable, highly soluble substances that are added into the system. Ideally a tracer is conservative, which means it does not react with the surrounding material of the aquifer and behaves the same as water. However, most artificial tracer are not conservative and their specific performance has to be taken into account. Information about catchment flow dynamics can be derived from the concentration dynamics of the tracer measured at the input versus the output location. (Goldscheider et al., 2008). The limiting factor of artificial tracers is the temporal and spatial extend that can be covered. Even if several tracers are applied only a few locations and a few flow states (such as storm events) can be covered. It limits the information gain to selected catchment state system dynamics (Beven, 2012). In karst systems artificial tracers are usually applied during high flow conditions, which provides information about short-term system reactions but insufficient information about the flow processes during dry periods (Mudarra, Andreo, Marin, et al., 2014). The alternative to artificial tracers are so called environmental or natural tracers that cover the whole catchment and the temporal dynamics of the system. These substances

or solutes are continuously added throughout the catchment either through precipitation or through reactions in the aquifer. They can be either environmental isotopes, hydrochemical substances or anthropogenic pollutants with a continuous diffuse source (Leibundgut et al., 2009). For all environmental tracers it is important to have a long period of time with measured data at the system output (e.g. spring discharge concentrations) and sometimes input (e.g. precipitation concentrations) as well. Ideally spring concentrations are measured continuously to cover the quick reactions of a karst system. If a continuous measurement is not possible, additional samples should be taken during relevant flow events (Hartmann, Goldscheider, et al., 2014; Mudarra and Andreo, 2011). The most common environmental tracers are isotope tracers such as $^{18}O/^{16}O$, $^{2}H/H$ and carbon isotopes. Especially for the application of transit time modelling isotope data is widely utilized (e.g. refer to McGuire and McDonnell, 2006). However, sometimes isotope data is not available, which is why hydrochemical tracers can be applied. An advantage of hydrochemical tracers is that they can deliver additional information about selected system processes like infiltration (Mudarra and Andreo, 2011), tributary mixing (Perrin et al., 2007), separation between different flow components (Lee and Krothe, 2003) and other. Dissolved ions in water can be used to estimate transit times, based on the concept of increased solute concentrations with continued contact time. Water with higher concentrations would imply a longer contact time and can therefore be associated with pre-event water versus water with low concentrations is more likely to be recent event water. A drop in mineralisation can be measured during high flow conditions, thus suggesting that more event water contributes to the discharge composition (Batiot, Liñán, et al., 2003; Goldscheider and Drew, 2007; Shuster and White, 1971). When dissolved ions are used as natural tracers it is recommended to use more than one solute, as different tracers can describe different aspects of the system, depending for example on the location of the source within the aquifer (Hartmann, Weiler, et al., 2013).
This is the reason why this study applies the new modelling framework to two different solutes, sulfate (SO_4^{2-}) and chloride (Cl^-). Both are common solutes in karst but originate from different sources within the system. They have been described to be conservative under karst conditions and are most common in systems with evaporite layers (Goldscheider and Drew, 2007). While SO_4^{2-} can enter the system through anthropogenic sources or in small amounts through precipitation its main source are gypsum or anhydrite. As equation 1.2 illustrates, if gypsum comes in contact with water, it exists in a state of chemical equilibrium with SO_4^{2-}. It has a maximum solubility of 2400 mg/l

at 25 °C and 1 bar (105 Pa) pressure (Ford and Williams, 2007). $SO_4{}^{2-}$ has been used as tracer in different studies (e.g. Klimchouk and Aksem, (2005);Lee and Krothe, (2003)). It can only be applied in catchments without sulfate input through thermal activity (Worthington and Ford, 1995).

$$CaSO_4 \cdot H_2O \rightleftharpoons Ca^{2+} + SO_4{}^{2-} + 2\,H_2O \tag{1.2}$$

Chloride (Cl^-) is a widely used tracer mineral as well (e.g. Harman, (2015), Hrachowitz et al., (2010), Kirchner et al., (2001), and Oda et al., (2009)). It enters the system through precipitation, anthropogenic sources or it can occur through geogenic dissolution of evaporites such as halite. Depending on the location a diffuse input through sea mist is also possible. Chloride concentrations in the uppermost storage layer, the soil-water zone, increase during the summer due to evaporation losses, the so called evapoconcentration effect (Ford and Williams, 2007). The geogenic source halite has a high solubility of 360 000 mg/l at 25 °C and 1 bar (105 Pa) pressure and dissolves into Cl^- and Na^+ as displayed in equation 1.3 (Ford and Williams, 2007).

$$NaCl + H_2O \rightleftharpoons Na^+ + Cl^- + H^+ + OH^- \tag{1.3}$$

Calcium (Ca^{2+}) is the most abundant solute in a karst catchment yet is not recommended as a tracer to estimate transit times. Its dissolution depends on the partial pressure of CO_2, which changes throughout the aquifer thus making a correlation between concentration and contact time infeasible. As karst systems are mainly made out of carbonate rock, even young water already has a high mineralisation regardless of contact time (Goldscheider and Drew, 2007). Batiot, Emblanch, et al., (2003) suggest to use magnesium (Mg^{2+}) as an indicator of transit time due to a slower dissolution rate, but Batiot, Liñán, et al., (2003) object that the correlation between Mg^{2+} and transit time can be dependent on the specific catchment and geology and might thus not be easily transferable.

Hydraulic and hydrological methods

Further methods to analyse karst systems include hydraulic and hydrologic approaches. A hydraulic examination of an aquifer can provide information about a number of pa-

rameters, which Goldscheider and Drew, (2007) cite as porosity, hydraulic head, transmissivity and hydraulic conductivity, groundwater velocity and groundwater flow rate. Methods applied to reach these informations are pumping tests, monitoring wells or borehole packer tests. The execution in karst areas is a challenge since test wells might miss water bearing layers or might be immersed into an underground reservoir, thus delivering distorted results. The spatial heterogeneity of a karst aquifer often leads to high conductivity rates, which reflect the high conductivity of the conduit system and not the conductivity of the whole aquifer including matrix and epikarst (Goldscheider and Drew, 2007; Kiraly, 1975). Hydrologic approaches to catchment characteristics of karst aquifers are a basic water balance concept and the analysis of spring hydrographs. A simple water balance of the form

$$\Delta S = P - (Q + ET) \tag{1.4}$$

with the precipitation P, discharge Q, evapotranspiration ET and the change in storage ΔS takes into account the gains and losses of the system and might indicate storage magnitude. While the calculation of the water balance might be simple, it is a challenge to accurately determine the input and output variables, as they can vary with flow conditions (Ford and Williams, 2007). The spatial heterogeneity of the system has the effect that depending on water table height additional overflow springs might be actived, which in turn changes the recharge area (Goldscheider and Drew, 2007; Hartmann, Barberá, et al., 2013). Boundary conditions need to be taken into account when calculating the water balance.

The spring hydrograph is the reaction of a catchment to precipitation events. Due to a quick flow component the reaction commonly occurs within a few hours to a few days depending on the system. Physical equations fit to the form of the discharge peak or recession curve offer estimates about storage, permeability, solute transport or transit times (Ghasemizadeh et al., 2012; Szilagyi et al., 1998; Tallaksen, 1995). Much like tracer information, discharge measurements are ideally available continuously to cover the temporal variability experienced in karst aquifers. High resolution discharge data is used as input for hydrological models as well.

Modelling of karst aquifers

While modelling groundwater flow and solute transport it is a common concept to determine catchment characteristics, most of the prevailing modelling techniques cannot be employed in karstic areas as Darcy's law does not apply in open flow conduits (Field, 1997; Ford and Williams, 2007). The duality in karst systems is a further challenge in modelling aquifer conditions due to the different velocities of flow, infiltration and storage components. Flow and storage conditions are similarly heterogeneous regarding water velocity and storage depletion (Ford and Williams, 2007; Ghasemizadeh et al., 2012; Sauter et al., 2006).

For that reason various models are currently applied which use different approaches for modelling groundwater flow and catchment behaviour in karstic areas. Most models can usually belong to one of two categories, either lumped parameter models (also called global models) and distributed models. Spatially distributed models divide the modelled area into grid cells covering either a two- or three-dimensional space, where each grid cell has their own characteristic parameter set and boundary conditions. For distributed models a number of different approaches have been developed to cover the spatial heterogeneity. From all distributive models the equivalent porous medium approach implements spatial variations the least, as it assumes averaged system properties for each modelled sub-unit. Therefore, it does not have the ability to represent the characteristics of the conduit system. The double continuum approach is able to cover both the conduits system and the matrix by simulating both as continua that interact (exchange of water and solute) with each other based on the difference in hydraulic head (Goldscheider and Drew, 2007; Hartmann, Goldscheider, et al., 2014; Teutsch, 1988). The combined discrete-continuum approach incorporates the advantages of both previous methods by merging discrete elements that represent conduit or fracture behaviour with a continuum that represents the matrix. Although data intensive, it is well suited to test theoretical karst models (Goldscheider and Drew, 2007; Kiraly, 1998). One example of a distributed model is the APLIS method to calculate recharge in karstic areas. It uses spatially distributed precipitation as input data and combines it with parameter values describing altitude, slope, lithology, infiltration landforms, and soil types for each grid cell (Andreo et al., 2008). The challenge for this data intensive method is to assemble the required information for the heterogeneous surface and subsurface conditions of a

karst aquifer (Ghasemizadeh et al., 2012). Nevertheless, it has the advantage of spatially distributed information about the recharge rate in the area of interest.

Another way to model catchment behaviour are lumped parameter models, which in some instances predict tracer output as good as as distributed model (Maloszewski and Seiler, 2000 cited in Ozyurt and Bayari, 2005, p.3269). In addition to flow rate calculation, lumped parameter models can be used to calculate recharge or simulate spring discharge as well as water levels (Ghasemizadeh et al., 2012). They are separated into two different types of model: black-box and grey-box models. Black-box models analyse a time series of input (usually precipitation) and output (discharge) data and try to find a transfer function between the two (Denić-Jukić and Jukić, 2003; Jukić and Denić-Jukić, 2006). No information about the catchment is assumed and the model only provides limited information about the physical properties of the study area (Goldscheider and Drew, 2007). The other type of model is the grey-box model, where some catchment characteristics are known and some are unknown (Deng, 1982). Hao et al., (2006), Ford and Williams, (2007) and others state that for karst aquifers the general flow processes like infiltration and flow through conduits or matrix are known and controlled by the meteorology, topography or the physical and geological structure of the catchment as well as influenced by vegetation and human activities. However, it is difficult to exactly quantify them by using mathematical models. Grey-box models are therefore appropriate for karst as they can use known parameters to explore unknown processes. Depending on the intended results lumped parameter models rely on the relationship between discharge and storage, based on the interpretation of discharge curves or chemical or hydraulic reaction of a spring to a precipitation event (Ghasemizadeh et al., 2012; Hartmann, Goldscheider, et al., 2014; Sauter et al., 2006). Since there is no need for extensive spatial data, which are often difficult to acquire, these kinds of models are generally preferred for karst catchments (Jukić and Denić-Jukić, 2009).

One example of a model which combines both distributed and global approaches is the semi-distributed VarKarst model developed by Hartmann, Barberá, et al., 2013 for a karst spring in southern Spain. The structure of the VarKarst model is displayed in Figure 1.3. It consists of N compartments where each compartment represents the properties of a piece of a cross section of the aquifer with varying thickness of soil, epikarst, diffuse groundwater, and concentrated groundwater systems. The combination of a cross section with a conceptual structure of the different layers allows to partially cover heterogeneity as well as anisotropy in the aquifer. Due to the varying input from

soil and epikarst, the recharge area that actually contributes to discharge varies and thus approaches reality in karst aquifers. After proving that it successfully models karst recharge, it was, inter alia, applied in combination with the distributed APLIS method (Andreo et al., 2008) to the Villanueva del Rosario catchment that is analysed in this study (Hartmann, Mudarra, et al., 2014).

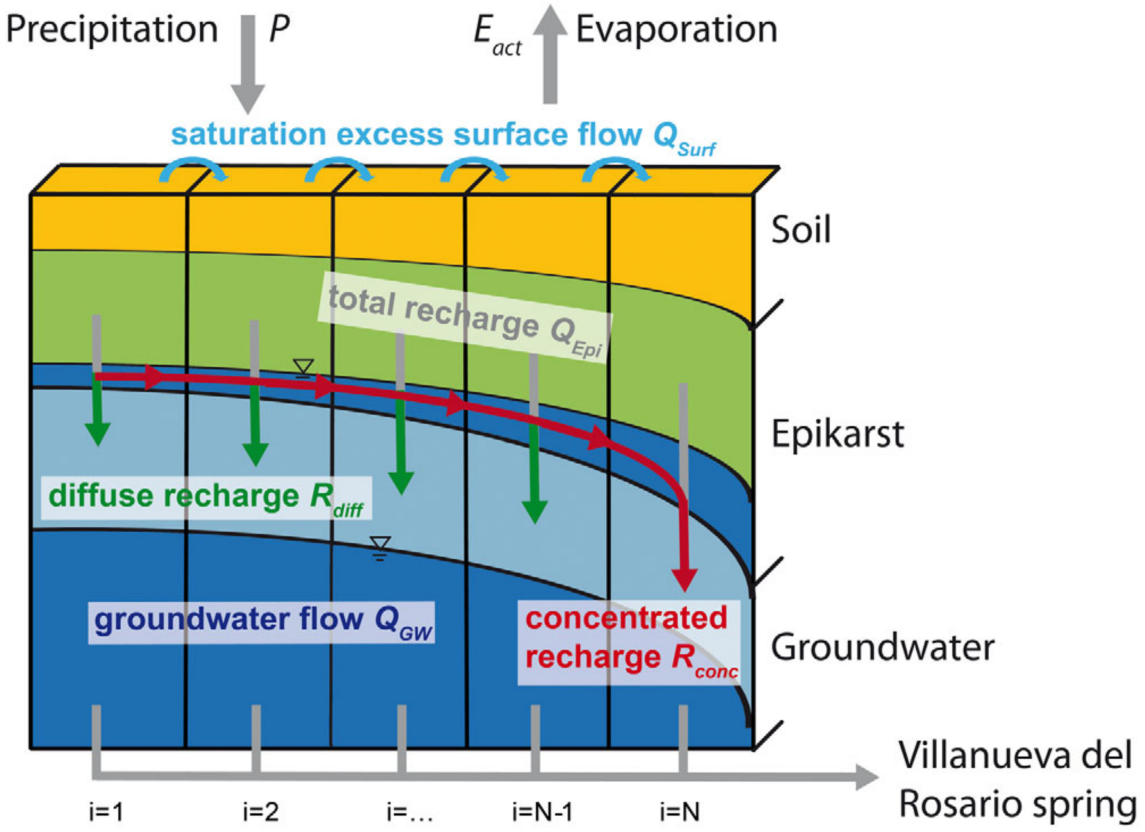

Figure 1.3: Diagram of the VarKarst model structure (Hartmann, Weiler, et al., (2013) modified by Hartmann, Mudarra, et al., (2014))

1.2.2 Transit times and StorAge Selection functions

Transit time

Tracer concentrations in the chemograph which are predicted by lumped parameter models rely on mixing between old and young water in the catchment which can be inferred

from transit time distributions (Amin and Campana, 1996; McGuire and McDonnell, 2006; Rinaldo et al., 2011; Sklash and Farvolden, 1979). The time water needs to travel through a catchment is called travel time (Botter et al., 2011) or more commonly transit time. It is not only a measure for a number of different catchment characteristics such as catchment storage, flow paths and water origin (Harman, 2015; McDonnell et al., 2010; McGuire and McDonnell, 2006), but is also a valuable source of information in case of contamination. It describes when the contaminant might reach a possible drinking water well and how long it will take until the catchment is cleared (Botter et al., 2011; Harman, 2015). Contrary to the concept of residence time, which describes the time a water particle spends inside a system until the time of observation, transit time is the time that has passed when the particle exits the system at the catchment outlet and thus includes overland and channel flow (Bolin and Rodhe, 1973; Etcheverry and Perrochet, 2000; Lindgren et al., 2004). Water travels from catchment input to catchment outlet at different velocities and through different flow paths. A sample of water that exits the system at a certain time has a probability density function of an "age" distribution which is called the transit time distribution (TTD).

Steady state versus time variable transit time distributions

The prevalent way lumped parameter models have been applied to determine tracer transport was to assume a steady state of the system with a time-invariant transit time distribution (Amin and Campana, 1996; Einsiedl, 2005; Maloszewski et al., 1992). The advantage of a time-invariant approach is the straightforward way to calculate the output from a linear process, if the input is known (Niemi, 1977). Time-variant functions on the other hand add a complexity to the calculation and interpretation of the results, which is the reason why it has not been a widely applied concept (McGuire and McDonnell, 2006). However, the temporal variation of input, output and storage volume leads to changes in catchment wetness and thus discharge variability, which influence the transit time in a way that cannot be neglected, as it has a significant effect on modelling results (Hrachowitz et al., 2013). The time it takes for a contaminant to leave the system depends substantially on the chosen function. It can vary between a few years in a steady-state case and a few decades for a time-variant model. The differences are particularly notable in a system with short mean residence times, such as karst (Harman, 2015; Ozyurt and Bayari, 2005). The reason for this is that a lower antecedent wetness might lead to longer

transit times, as the hydraulic conductivity decreases (McGuire and McDonnell, 2006). The high variability of flowpaths controlled by catchment form and storage volume is especially relevant for karst catchments. During heavy precipitation events faster flow paths are not only added by overland storm flow but also through additional usually dry flow paths in the form of sinkholes which become active and add a much quicker, concentrated flow component. Changes in the groundwater level can further add overflow springs or change the recharge area (Hartmann et al., 2012; White, 2002). McDonnell et al., (2010) additionally pointed out that non steady-state conditions mainly occur in small catchments with a highly variable storage volume. This applies especially for karst which has a dynamic storage (Jacob et al., 2008; Jacob et al., 2010; Maloszewski et al., 2002). Although Niemi, (1977) was one of the first authors to recognise that a change in storage size can influence catchment reactions, time-variant transit time distributions have only recently been applied (Benettin, Kirchner, et al., 2015; Botter et al., 2010; Botter et al., 2011; Harman, 2015; Hrachowitz et al., 2010; Rinaldo et al., 2011; van der Velde et al., 2012). Before that there were different approaches to apprehend tracer response in the output signal that could not be explained with a single steady-state TTD, by assigning separate assumed steady-state distribution for different flow states or flow components (Lee and Krothe, 2001; Stumpp et al., 2009; Weiler et al., 2003).

StorAge Selection functions

It has been established that water travels through the system at different velocities and flow paths which are influenced by time variable catchment conditions such as antecedent wetness. However, this implies that discharge at catchment outlet consists of a mix of older and younger water. In karst catchments water mobilised after a storm event originates from different parts of the storage and mixes in the spring, thus producing a varying tracer signal (Bakalowicz and Mangin, 1980; Lakey and Krothe, 1996; Sauter, 1997). For different catchments this reaction varies. In some catchments the discharge after a storm is mainly event water, due to increased overland flow for example (Heidbüchel et al., 2013; Morgenstern et al., 2010; Segura et al., 2012), but in others discharge is in parts or completely older water, which has been stored in the system for a longer time. This effect is called the ”old-water paradox” (Birkel et al., 2012; Klaus and McDonnell, 2013; Rinaldo et al., 2015). To consider the ability of a catchment to

store and mix water as well as solutes a new approach was developed by Botter et al., (2011) and improved by van der Velde et al., (2012) and Harman, (2015).

The residence time distribution (RTD) $p_S(T,t)$ describes the age distribution in the storage. It is defined as

$$p_S(T,t) = \frac{S_T(T,t)}{S(t)} \tag{1.5}$$

where $S_T(T,t)$ is the storage at time t older than age T and S(t) the total storage at time t (Botter et al., 2011; Harman, 2015; van der Velde et al., 2012). While the residence time distribution (RTD) describes the current state of the storage, TTDs describe the age distribution as water exits the system. They can be differentiated into a forward transit time distribution (fTTD) and a backward transit time distribution (bTTD). The fTTD described as $\overrightarrow{p}_Q(T,t)$, defines the "age" T of water leaving the system over an extended period of time, which entered on the same time t_i. The bTTD or "reverse travel time distribution" on the other hand (van der Velde et al., 2010) describes the "age" T of water particles entering the system over an extended period of time and leaving as discharge at the same exit time t. The backward transit time distribution is defined as:

$$\overleftarrow{p}_Q(T,t) = \frac{Q_T(T,t)}{Q(t)} \tag{1.6}$$

where $Q_T(T,t)$ is the discharge at time t older than age T and Q(t) the total discharge at time t (Botter et al., 2011; Harman, 2015; van der Velde et al., 2012). The bTTD of water particles leaving the system via evapotranspiration is described respectively as:

$$\overleftarrow{p}_{ET}(T,t) = \frac{ET_T(T,t)}{ET(t)} \tag{1.7}$$

The definition of a bTTD is mostly used in the area of chemical engineering where it is called the "exit age distribution" (Danckwerts, 1953; Harman, 2015; Levenspiel, 1999; Rinaldo et al., 2015). The advantage of using a reverse TTD is that it allows to predict the tracer concentration in the output by knowing the input tracer concentration (Harman, 2015; Rinaldo et al., 2011).

$$C_{out}(t) = \int_{-\infty}^{t} C_{in}(t_i)\ \overleftarrow{p}_Q(T,t)\ \mathrm{d}t_i \tag{1.8}$$

The forward transit time distribution described as $\overrightarrow{p}_Q(T,t)$ and backward transit time distribution do not take the same functional form unless constant input/output

conditions (steady-state) are assumed (Niemi, 1977). While artificial or natural tracer experiments generate fTTD for the time t_i, bTTDs can not, or only at great effort, for example by using multiple tracers (McDonnell et al., 2010), be determined from tracer breakthrough curves. Instead their functional form is determined through lumped parameter models or derived from the observed change in natural tracer signals (Kirchner et al., 2000).

Botter et al., (2011) was the first to establish a connection between bTTD and the residence time distribution $p_S(T,t)$ as the water removed from the system through the bTTD is directly dependent on the water age distribution that is available for removals as described by the RTD. They established a Master Equation, which describes the connection between RTD and bTTD. The transformation between storage with a known age-distribution into discharge with a known age distribution is expressed as what Botter et al., (2011) called a "mixing function" and what is since then known under the more established term StorAge Selection (SAS) function (Rinaldo et al., 2015). For the two fluxes discharge Q and evapotranspiration ET the SAS is written in the notation by Rinaldo et al., (2015) as:

$$\omega_Q(T,t) = \frac{p_Q(T,t)}{p_S(T,t)} \tag{1.9}$$

$$\omega_{ET}(T,t) = \frac{p_{ET}(T,t)}{p_S(T,t)} \tag{1.10}$$

Harman, (2015) explains the complication associated with this approach. The parameters to describe $\omega_Q(T,t)$ can only be determined for a simple case, as $p_S(T,t)$ depends on the full, partly unknown history of input fluxes into the system. Due to this reason van der Velde et al., (2012) further developed the framework by selecting the discharge not from the RTD but from the cumulative probability of the residence time distribution. The advantages detected by van der Velde et al., (2012) are an easier parametrization, an improved interpretation of the parameters in terms of actual mixing behaviour in the aquifer, and more consistency in time.

Harman, (2015) adopts a similar approach by applying the selection function to the new variable age-ranked storage $S_T(T,t)$ [mm]. The approach is described in more detail

in section 3.3. The age-ranked storage is defined in relation to the cumulative RTD ($P_S(T,t)$) and total storage as:

$$S_T(T,t) = S(t)\ P_S(T,t) \tag{1.11}$$

In agreement with Botter et al., (2011), van der Velde et al., (2012) and Harman, (2015) the SAS framework $\omega_Q(T,t)$ is referred to as "absolute" StorAge Selection (aSAS) function, $\omega_Q(P_S,t)$ is referred to as "fractional" StorAge Selection (fSAS) function and the new approach $\omega_Q(S_T,t)$ is referred to as "rank" StorAge Selection (rSAS) function.

The advantage of rSAS is that it does not require knowledge about the total storage volume, which is often difficult to determine, but can instead be applied to the active part of storage. This further means that no lower system boundary needs to be assumed, thus reducing the risk of errors (Harman, 2015). The main advantage is its ability to include a catchment state variable, which influences transit time distribution and describes their temporal variability. This can be storage, but other state variables such as water level or discharge can be chosen as well (Harman, 2015; Rinaldo et al., 2015). rSAS has been developed and tested at the Lower Hafren catchment in Wales. It was possible to predict chloride transport dynamics in the discharge by applying a storage-dependent gamma distribution as selection function. The age composition of the discharge, derived from the chloride transport, showed a connection to the moisture content of the catchment. During a state of low storage the discharge is mainly composed from pre-event water. This was termed the "inverse storage effect" (Harman, 2015). Since then the rSAS framework has been applied to a sloping lysimeter, in an attempt to measure TTDs experimentally (Kim et al., 2016), and to a small stream under baseflow conditions to model sequential tracer injections (Harman et al., 2016).

Harman, (2015) and Rinaldo et al., (2015) theorize that the rSAS/SAS framework is flexible enough to potentially be applied to a flow system independent of its structure, which would make it a widely applicable tool. The spatial heterogeneity of the chosen catchment which results in multiple different flowpaths is taken into account by the flexibility of the selection function, which regards the water input over the complete system.

2 Problems and objectives

The hypothesis for this study is that the rSAS model developed by Harman, (2015) fulfils all the prerequisites to perform well even in a catchment with a complex flow regime such as karst. The assumption to be tested is that the application of a time-variable StorAge selection function to an age ranked storage (rSAS) is well suited to calculate solute transport in karst. It has been recommended by Harman, (2015) and Rinaldo et al., (2015) to test the new SAS theory on different flow systems to prove their assumed broad applicability. Harman, (2015) further recommended to test the model in different landscapes to see if a connection between the parameters and the physical structure of the catchment can be established. Although this is not discussed as part of this thesis, as only one catchment is analysed, this work adds to the experience with rSAS and the general SAS theory. This work incorporates not yet published further enhancements by Ciaran Harman to the rSAS model in the form of an enrichment function to model geogenic dissolution as tracer input. They were developed to adapt the model to the specific requirements for solute transport in karst aquifers. Neither the SAS framework in general nor the rSAS model has been applied to a karst catchment before. If it performs well, it could support the management of drinking water resources in regard to the risk of contamination as an less data intensive transport model. Commonly used lumped parameter models have furthermore been described to be error prone in karst areas as they are limited in the display of the aquifer heterogeneities (Ford and Williams, 2007; Palmer, 1999). The application of rSAS as a first assessment of the aquifer or in combination with lumped parameter models might be able to reduce uncertainty and errors in modelling. In connection to the results delivered by rSAS for this specific catchment an additional question is discussed during the scope of the thesis: Is the rSAS model a black-box model, that does not assume any parameter information or can it be regarded as a grey-box model as it provides information about the catchment processes and takes the physical structure of the catchment into account? The hypothesis is that rSAS can be classified as a grey-box model. To prove or disprove both hypothesis a

catchment in northern Spain is modelled with rSAS. It qualified as study area since it has been investigated extensively regarding the hydrology, geology and flow system. The application of a transport model is of interest for that specific area, as the spring supplies a small village with drinking water. The success of the rSAS model is determined by comparing it against the benchmark model VarKarst, which has been applied to the study area as well (Hartmann, Barberá, et al., 2013) and to the results of previous tracer experiments (Mudarra and Andreo, 2011; Mudarra, Andreo, Marin, et al., 2014).

3 Methods

3.1 Study area

The Alta Cadena mountain range is based in southern Spain, close to Malaga City and is drained by multiple Karst springs. One of them is Rosario spring, which drains the Villanueva del Rosario Karst system located in the middle of the Alta Cadena massif. The recharge area of Rosario spring, depicted in Figure 3.1 is approximately 13.85 km^2 as determined by several studies (Marin et al., 2010; Mudarra, Andreo, Marin, et al., 2014; Hartmann, Mudarra, et al., 2014). The main geologic feature of the catchment is limestone with some small patches of clays and sandstone close to the surface. While there are some large areas of underlying dolostone they rarely reach the surface. Upper Triassic clays and evaporite rocks, in the form of gypsum, are located below the roughly 400-450 m of limestone and dolostone and are a source of $SO_4{}^{2-}$ in the spring discharge. Traces of halite in the area lead to the input of Cl^- into the spring water (Martín-Algarra, 1987; Hartmann, Mudarra, et al., 2014; Mudarra, Andreo, Marin, et al., 2014; Peyre, 1974). The relief is rugged with altitudes rising from 600 to 1640 m above sea level (ASL). The vegetation is dominated by light patches of pasture and shrubs with scattered areas of bare soil. There are some forested areas and a few olive and nut tree plantations. Occasional livestock farming leads to a slight nitrate ($NO_3{}^-$) input into the spring. The catchment receives 760 mm of mean annual precipitation (Mudarra, Andreo, Barberá, et al., 2014) with a distinct wet season during the fall, winter and spring and a dry period during the summer months. Rosario spring is located at the north west corner of the catchment at 755 m ASL, where it discharges the karstified Rosario catchment (Mudarra, Andreo, Barberá, et al., 2014). A tracer test done by Martínez et al., (2010) proved the karstic behaviour of the catchment. Karstic landscape features of the area are karrenfields, dolines, uvalas and swallow holes, which are triggered during large storm events (Hartmann, Mudarra, et al., 2014). The catchment reacts quickly to precipitation

events with a fast flow component that reaches velocities of up to 200 m/h (Martínez et al., 2010).

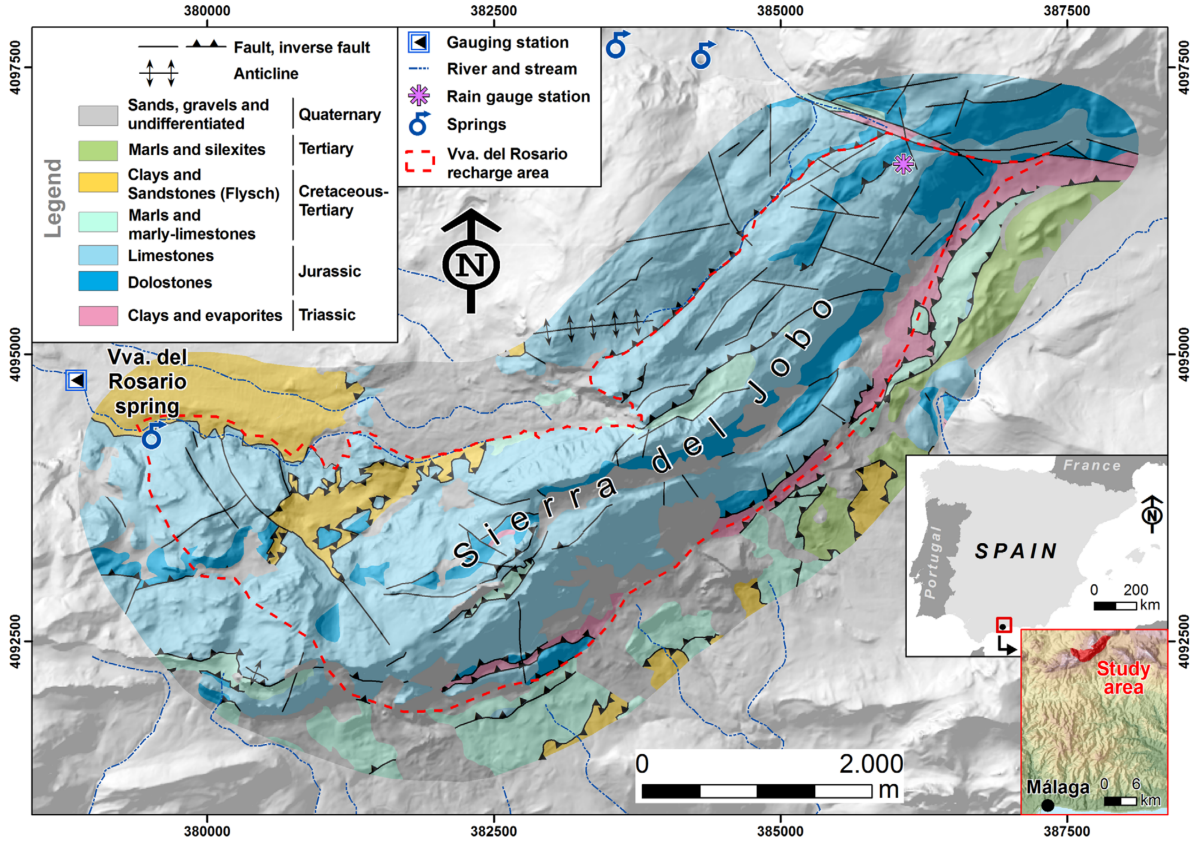

Figure 3.1: Map of the geology and recharge area of the Villanueva del Rosario catchment, including the location of the spring and gauging station as well as the general location of the catchment in Southern Spain (Hartmann, Mudarra, et al., 2014)

3.2 Data

The data used in this study was collected by Mudarra and Andreo, (2011) and Mudarra, Andreo, Barberá, et al., (2014) between October 2006 and September 2009. The same data was used in the application of the benchmark model VarKarst (Hartmann, Mudarra, et al., 2014). It was checked for completeness, but was assumed to be already interpolated to the study area. During the study period discharge, electrical conductivity

(EC) and water temperature (T_W) of Rosario spring and precipitation were continuously recorded and aggregated to daily mean values (discharge) and daily sums (precipitation). The precipitation station was located in the North-West of the study area (Figure 3.1) at 1,130 m ASL. The input hydrochemistry was measured in 31 irregular precipitation bulk samples over the three years. Discharge hydrochemistry was measured more regularly at a weekly interval during the rainy season and biweekly intervals during the dry season. Additional samples were taken during high flow conditions. The last precipitation sample was taken on 29.09.2009. The last discharge sample was taken earlier on 25.03.2009. The solutes and hydrochemistry parameters measured in precipitation and discharge were: ALK, Ca^{2+}, Cl^{-}, F^{-}, K^{+}, Na^{+}, Mg^{2+}, $NO_3{}^{-}$, and $SO_4{}^{2-}$. Furthermore, pH, $logP_{CO2}$, and $SI_{calcite}$ were measured solely in the discharge. rSAS requires continuous input concentrations. The precipitation bulk sample results were therefore assigned to all days, with values reaching backward until the previous sample. Another requirement is that there cannot be any solute input, if there is no water input. Therefore, on days with zero precipitation input concentration was set to zero as well (Harman, 2015). If it was not already the case in the original data, all concentrations were converted to mg/L. Discharge was converted from l/s to mm/d using the recharge area given by (Hartmann, Mudarra, et al., 2014) of 13.85 km^2.

Actual evapotranspiration data was taken from Kirn et al., (2016). They calculated potential evapotranspiration (PET) from temperature data using Thornthwaite's method (Thornthwaite, 1948) and entered it into a simple soil routine to compute actual evapotranspiration (AET). The MODIS (Moderate-resolution Imaging Spectroradiometer) evapotranspiration data set was considered as well. It relies on satellite measurements of land cover, leaf area index, air temperature, pressure and humidity and radiation, which are used to compute plant and soil evaporation for a 1 km x 1 km grid and 8-day time frame (ORNL DAAC, 2008). Both ET datasets were compared to the ET determined by the VarKarst model. The soil routine ET was closer to the benchmark model and was therefore chosen for the simulations to model with similar initial conditions .

There was no isotope data availabe for the study period, which is why two solutes were chosen as tracer. Chloride (Cl^{-}) is a solute that has previously been used in different models (e.g. Hrachowitz et al., (2010), Kirchner et al., (2001), and Oda et al., (2009)). Harman, (2015) used Cl^{-} to compute solute transport when he developed the rSAS model and applied it to a catchment in Plynlimon, Wales. Chloride input into the Rosario system originates from precipitation as well as geogenic dissolution. It can

therefore be considered to enter the system from the surface as well as over the whole depth of the aquifer. Sulfate ($SO_4{}^{2-}$) on the other hand mainly enters the system through geogenic dissolution. The source, gypsum, is located deeper in the aquifer and can thus provide information about the deeper flow system. The two solutes were analysed separately to preserve the information gained from the different locations within the aquifer (Hartmann, Weiler, et al., 2013).

3.2.1 Storage estimation

The time variable transit time distribution of the rSAS model varies with a state variable. This state variable should represent a catchment parameter which influences the transit time. Harman, (2015) suggests to use the catchment storage, as flow conditions change with different states of wetness. Since this applies for karst catchments as well, storage was chosen as the state variable (Hartmann et al., 2012; McDonnell et al., 2010; White, 2002). A method to calculate changes in catchment storage is to use a simple water balance equation, where storage change is the difference between fluxes in (precipitation P) and fluxes out (evapotranspiration ET and discharge Q), as seen in equation 3.1. The storage estimation does not calculate actual storage but instead represents the hydrologically active part of storage, thus leaving out water which does not partake in the flow regime. In order to not assume any prior knowledge about storage levels the starting value of the storage is set to zero. The calculated changes in storage are added up with each time step. The cumulative sum of all previous time steps is assumed to be the storage at the current time step. With a base value of zero negative storage values are possible and do not imply an actual negative storage. It would have been possible to add a set value to the calculated storage, which would have increased it enough for all values to be positive. However, this would have implied that the lowest storage values calculated during the study period are actually the lowest storage values possible. To not make this assumption a base value of zero is assumed, which is not restricted to a lower limit.

$$\Delta S = P - ET - Q \tag{3.1}$$

3.3 rank StorAge Selection

Harman, (2015) developed the concept of an age-ranked StorAge Selection function (rSAS) to predict transit times and thus solute transport in a system. It extents theories by Botter et al., (2011) and van der Velde et al., (2012). An outline of the framework described by Harman, (2015) and taken further by Harman et al., (2016) is presented here. A more detailed description can be found in the respective papers.

The theoretical background of the model is the transport through a control volume with defined boundaries, which can for example be a catchment, river or a lysimeter as long as input and output conditions are known. $S_T = S_T(T,t)$ is defined as the new variable age-ranked storage, where the water volume at time t is aged less than age T. S_T can be expressed as

$$S_T(T,t) = S(t) * P_S(T,t) \tag{3.2}$$

if the total storage is known. A similar variable $Q_T(T,t)$ can be defined for the discharge which leaves at time t with an age less than T. It is the un-normalized expression of the transit time distribution.

$$P_Q(T,t) = S_T(T,t) * S(t) \tag{3.3}$$

As the total storage is difficult to quantify, S_T can be calculated without knowledge of the actual storage by applying the conservation law:

$$\frac{d}{dt}S_T(t-t_i,t) = \frac{\partial S_T}{\partial T} + \frac{\partial S_T}{\partial t} = J(t) - Q_T(T,t) - ET_T(T,t) \tag{3.4}$$

The storage at time t consists of water younger than age T, that has not been removed so far. The change in storage is described by adding the input J(t) (here called J to distinguish from the TTD notation), which has an age of zero and the removal of water through discharge or evapotranspiration. The water that is removed has a specific age distribution. The age distribution, described by the transit time in form of water age, can also be described in form of S_T instead, as T and S_T are connected by the monotonically increasing water age. The new function $\Omega_Q(S_T,t)$ equals the transit time distribution $P_Q(T,t)$, when $S_T = S_T(T,t)$. This cumulative distribution is the actual rank StorAge Selection function and represents a probability distribution over the storage (Harman et al., 2016). To obtain the probability density function (PDF) of the rSAS function, a

derivative is taken over the transit time distribution and rSAS function, which allows to express the transit time distribution in terms of storage instead of age:

$$p_Q(T,t)\partial T = \omega_Q(S_T,t)\partial S_T \tag{3.5}$$

for $S_T = S_T(T,t)$. If input and output into the system as well as the rSAS function $\Omega_Q(S_T,t)$ are known, it is possible to calculate the time-variable transit time distribution. With a known tracer inflow concentration it can be used to calculate outflow concentration, as mentioned in section 1.2.2, Equation 1.8. For the functional form of Ω_Q (Harman, 2015) suggests to refer to the properties of the associated TTD. The comparison between a uniform and a gamma distribution as rSAS function to describe discharge age revealed that the gamma distribution returned better results as it was better able to cover the age variability of the Plynlimon catchment (Harman, 2015). Kirchner et al., (2000) and Hrachowitz et al., (2010) both proved that the flexibility of a two parameter gamma function covers mixing processes in the catchment and is a good representation of transit time distributions. The rSAS function is therefore defined as:

$$\Omega_Q(S_T,t) = \frac{\Gamma^{\alpha-1}}{\beta^\alpha \Gamma(\alpha)} e^{-S_T \backslash \beta} \tag{3.6}$$

with α as a shape parameter and β as a scale parameter. While the external variability of the system is taken into account by using time-variable in- and outflows, the internal variability can be included by using a time-variable β parameter. It is defined as:

$$\beta = \frac{\lambda}{\alpha}(\Delta S - \Delta S_{crit}) \tag{3.7}$$

where λ is described as a fitting parameter and dS_{crit} as the critical storage. The state variable, which introduces the time-variance is the storage S. If the storage passes critical storage, only event water is sampled for the discharge. The parameter influences how much young water contributes to discharge composition. The closer the storage is to the critical storage, the more recent event water is sampled. The parameter were determined by applying an optimization approach to find the best model prediction. The evapotranspiration flux out of the system was sampled through a SAS function as well. According to Harman, (2015) a uniform distribution represents evapotranspiration from the age-ranked storage. In addition a time-invariant model run with a *beta* parameter

defined through optimization was done for SO_4^{2-} to briefly compare the time-variant and time-invariant approach.

The solute transport calculations applying rSAS were done using the rSAS library by Harman, (2016). The model specific parameters were defined according to a general implementation. A warm-up period was not included in the calculations, as no data suitable for a rSAS were available. The use of the actual three years of data as warm-up would have started the calculations with elevated solute concentrations, due to the long dry period in the summer 2009. The use of average values of the three years on the other hand, would have resulted in a distorted relationship between concentration in storage and concentration in discharge.

3.4 Enrichment function

To model the geogenic dissolution of minerals as source of tracer solutes an enrichment function is included in the model comparable to the approach used by Benettin, Bailey, et al., (2015), where it was used to calculate dissolved silicon and sodium concentrations. Benettin, Bailey, et al., (2015) applied a simple first order reaction rate. The concentration of the solute (C(T)) in Equation 3.8 is dependent on the contact time (T) between source and fluid, the equilibrium concentration (C_{eq}) and the reaction rate (k1) (Benettin, Bailey, et al., 2015; Maher, 2011; Mercado and Billings, 1975).

$$C(T) = C_{eq} * (1 - e^{(-k1*T)}) \tag{3.8}$$

With a small change the method can be included into the rSAS model. rSAS calculates for every water parcel the time it spends inside the system in the form of a transit time distribution. Location within the aquifer and temperature changes during the year can be neglected for the calculation of geogenic dissolution (Botter et al., 2010; Ford and Williams, 2007). Benettin, Bailey, et al., (2015) assume an initial concentration of zero in the fluid, where solutes enter entirely through geogenic dissolution. Both solutes in this study, Cl^- and SO_4^{2-}, enter the system through precipitation as well as geogenic dissolution, Equation 3.8 was therefore modified (Equation 3.9) to include an initial concentration (input concentration (C_{in})). Input into Equation 3.9 is water age, $T = t - t_i$ (T), which is expressed through the PDF of the backwards transit time distribution and the input concentration. The parameters which are fit during the optimization process

are the reaction rate (k1) and the equilibrium concentration (C_{eq}), which is the limit that is approached by the exponential function. Another optimization parameter is the background concentration (C_{back}). At the start of the modelling period the concentration in the storage is unknown, but plays a significant role in the composition of discharge as the majority of the water is sampled from this undefined storage. To reduce the error a uniform background concentration is assumed, which ages with time the same way as the input water parcels. The enrichment function was included into the current version of the rSAS library (Harman, 2016).

$$C(T) = [C_{in}(t) * e^{(-k1*T)}] + [C_{eq} * (1 - e^{(-k1*T)})] \tag{3.9}$$

3.5 Model calibration and evaluation

To find the best parameter set, the function "fmin" of the Python (version 2.7.12) package "scipy" is applied (Nelder and Mead, 1965; Wright, 1996). It utilises a Nelder-Mead simplex algorithm to find the local minimum of the objective function. In this case the Euclidian distance (ED) between the simulated and observed output concentration as defined in equation 3.10 is used as the objective function during the optimization process. An optimal ED is close to zero (Gupta et al., 2009).

$$ED = \sqrt{(r-1)^2 + (\alpha-1)^2 + (\beta-1)^2} \tag{3.10}$$

with

$$\alpha = \frac{\sigma_s}{\sigma_o} \qquad \beta = \frac{\mu_s}{\mu_o} \tag{3.11}$$

r is here the linear correlation coefficient between simulate and observed solute concentration in discharge, σ_s/σ_o and μ_s/μ_o are the mean and standard deviation between simulated and observed values. The ED is part of the commonly used Kling-Gupta efficiency (KGE) (Gupta et al., 2009) and is defined as

$$KGE = 1 - ED \tag{3.12}$$

The ED was chosen as the objective function since the KGE in contrast to the ED is an efficiency measure that is maximized not minimized as requested by the optimization algorithm. To compare the modelling results with the results by Hartmann, Mudarra,

et al., (2014) the more common KGE with an aspired value close to one is calculated for the optimal parameter set determined by the optimization as well. It is also used for the calculation of the Generalized likelihood uncertainty estimation (GLUE) and the Hornberge-Spear-Young (HSY) sensitivity estimation. The algorithm runs with the starting parameters displayed in Table 3.1. As they are only the starting values for the optimization algorithm they are the same for both solutes.

3.5.1 Hornberger-Spear-Young method

Spear, (1980) developed the so called HSY method to detect sensitive parameters in a model (Beck, 1987). In preparation for the HSY method a Monte Carlo simulation with 30 000 runs was completed, where the parameter values were each randomly chosen from a uniform distribution. The boundaries of the uniform distribution were set to ± 75 % for the upper/lower limit of the optimized parameter value returned by the Nelder-Mead simplex algorithm. An exception was made for the upper limit of k1 and for the alpha (α) parameter. Previous HSY analysis showed that the relevant parameter space for k1 may vary by one power of ten. Similar effects took place for the α parameter, which caused an unstable model where $\log(\alpha)$ fell below -2. To compare both solutes assumed parameter limits were kept the same, although the Cl^- model found an optimised value of less than two. According to Beven, (2012) parameter bounds can be chosen based on previous knowledge to include good model fits or to exclude infeasible model runs. The number of runs were limited to 30 000 runs by available computing capacity and computing time. For each run the respective parameter set, efficiency value and simulated solute concentration were saved. The model runs were separated into behavioural and non-behavioural runs. The two solutes were modelled separately and reached different levels of efficiency in the rSAS model as well as the benchmark model. The binary classification rule takes these differences into account, by not using a fixed KGE value. Instead the 500 model runs with the highest KGE were declared as behavioural and compared to the non-behavioural model runs. For each parameter and parameter value the efficiency is normalised by calculating the likelihood value (L_i) of the parameter value using Equation 3.13. Based on this the empirical cumulative distribution function (eCDF) can be plotted for both groups.

$$L_i = \frac{KGE_i}{\sum KGE} \tag{3.13}$$

A parameter is determined sensitive, if a Kolmogorov–Smirnov test (KS test) finds a significant difference ($p<0.05$) between the eCDF of the behavioural and non-behavioural model runs. In addition to the p-value the KS test calculates the maximum absolute difference between behavioural and non-behavioural, called the D statistic (Massey, 1951). Based on the D statistic a relative difference in sensitivity can be assumed (Beven, 2012) and allows to sort sensitive parameters into three categories. Considering a p-value ≤ 0.05, a D value >0.2 indicates a high sensitivity, a D statistic between 0.2 and 0.1 a medium sensitivity and a D statistic <0.1 a low sensitivity. Parameters with a p-value >0.05 are deemed to be not sensitive.

Table 3.1: List of parameters with upper and lower Monte Carlo parameter ranges for SO_4^{2-} and Cl^- and initial parameter values for the Nelder-Mead algorithm (Start)

Parameter	Description	Unit	SO_4^{2-}		Cl^-		Start
			Lower	Upper	Lower	Upper	
C_{back}	background concentration	[mg/l]	10	68	7	49	50
k1	reaction rage	[mg/(l*d)]	0.0003	0.0100	0.0002	0.0100	0.001
C_{eq}	equilibrium concentration	[mg/l]	48	338	20	140	90
log(α)	shape parameter	[-]	-2	0	-2	0	-1.6
lambda (λ)	lambda	[-]	-2	-0.34	-2	-0.28	-1.5
critical storage (dS_{crit})	critical storage	[mm]	67	469	64	450	200

3.5.2 Generalized likelihood uncertainty estimation

To identify equifinality in the rSAS model a Generalized likelihood uncertainty estimation is performed. It builds on the concept by Beven and Binley, (1992) that several different parameter sets can reach an equally good fit to the observed data. Thus, single parameter should not be evaluated by itself, instead the results of different parameter sets have to be compared. The model output concentration for each behavioural parameter set from the Monte Carlo simulations, split with the same binary classification rule,

is used to calculate the prediction range for each time-step. A 95 % confidence interval denotes the predictive uncertainty.

3.5.3 Comparison to VarKarst

To test the performance of the new rSAS method the simulated vs. observed discharge concentrations of SO_4^{2-} and Cl^- are compared to the simulation results of the VarKarst model (Hartmann, Barberá, et al., 2013). The VarKarst model was applied to the same catchment and time frame (Hartmann, Mudarra, et al., 2014) and will therefore be considered as the target modelling performance that rSAS should reach or surpass to qualify as an acceptable new method. The modelling performance is assessed by comparing the KGE of both models for SO_4^{2-} and Cl^- as well as a visual comparison of the simulate versus observed values of both models.

4 Results

4.1 Hydrology

The Villanueva del Rosario catchment received a mean annual rainfall of 752 mm between October and September (hydrologic year) during the years 2006/2007 - 2008/2009, which was close to the mean historic annual precipitation of 760 mm. There was a high interannual variability between the three years. While the hydrologic years of 2006/2007 and 2007/2008 were comparatively dry with 642 and 682 mm respectively, 2008/2009 could be considered a wet year with 932 mm of precipitation. The corresponding discharge during the wet year was elevated as well with 692 mm during 2008/2009 and only 307 mm and 174 mm for the years 2006/2007 and 2007/2008. The low discharge values in 2007/2008 were a result of high AET values (referred to as ET from here on) during that year of 447 mm compared to 397 mm and 350 mm during the years 2006/2007 and 2008/2009. Spring discharge reacted quickly to precipitation events, as can be seen in Figure 4.1. A cross-correlation between discharge and precipitation showed two correlation peaks at one day lag and at four day lag both with a correlation coefficient of 0.32. The evapotranspiration calculated through a soil routine was highest in the second year with a total of 447 mm. This is partly due to a first peak in ET in October, followed by the regular peak at the end of spring. ET was lowest in the wet year with 350 mm. The first year had a total evapotranspiration of 397 mm. In general, precipitation peaks at the end of spring and drops during the summer months. The error in the water balance amounted to -61 mm, 62 mm and -109 mm. A comparison between ET calculated through VarKarst, ET calculated with the soil routine and satellite measured ET values by MODIS suggested that the MODIS ET values are too low, which would introduce an even greater error into the water balance and would have lead to a stronger storage accumulation (Figure 6.1 in the Appendix). The evapotranspiration returned by VarKarst was similar to the ET calculated through the soil routine. The storage calculated from

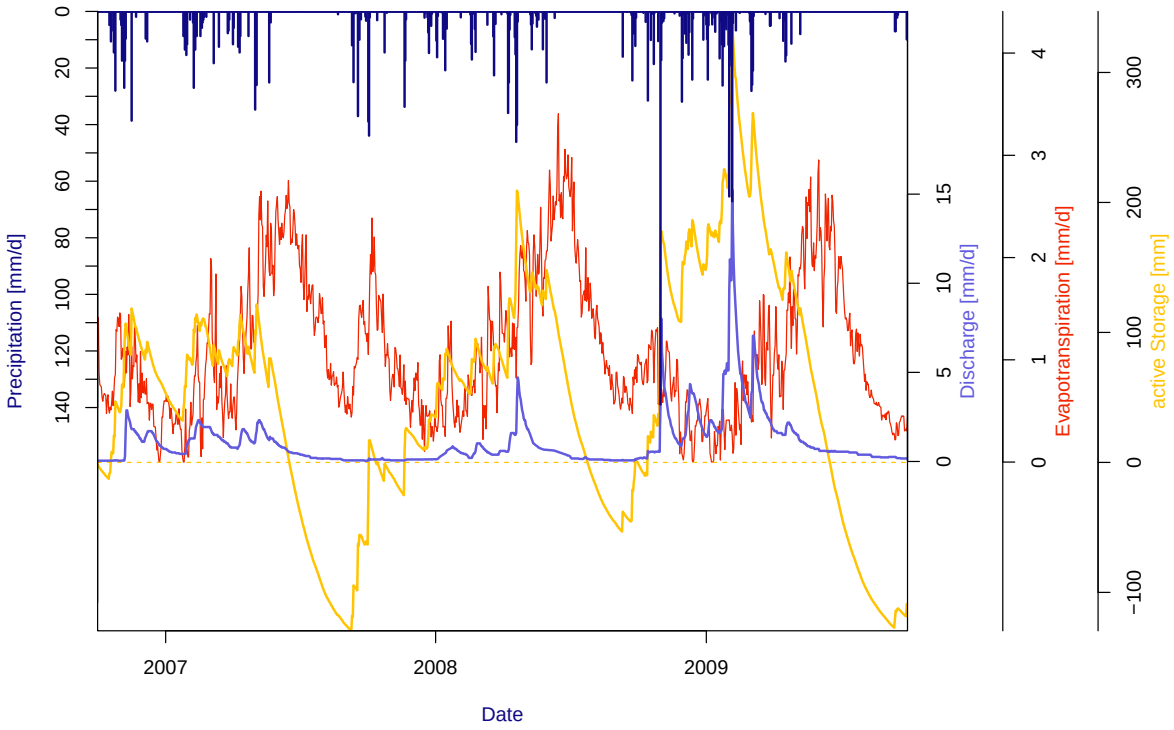

Figure 4.1: Time series of precipitation, discharge, actual evapotranspiration (ET) and storage in the Villanueva del Rosario catchment.

the three input and output variables P, Q and ET, with an initial value of zero, peaked at 121 mm in 2006/2007, 209 mm in 2007/2008 and 336 mm in 2008/2009. Figure 4.1 illustrates the increase in storage during the winter and the decrease during the summer. A comparatively short precipitation-free period in 2008 resulted in high storage values at the beginning of the wet season. The addition of a strong precipitation event in November 2008 lead to high storage values in 2008/2009.

4.2 Hydrochemistry

Of the available data two solutes were used for the application of rSAS. Input concentration for sulfate ranged from a minimum of 0.28 mg/l to a maximum of 2.23 mg/l with a daily mean concentration of 1.2 mg/l on days with precipitation. All non-precipitation

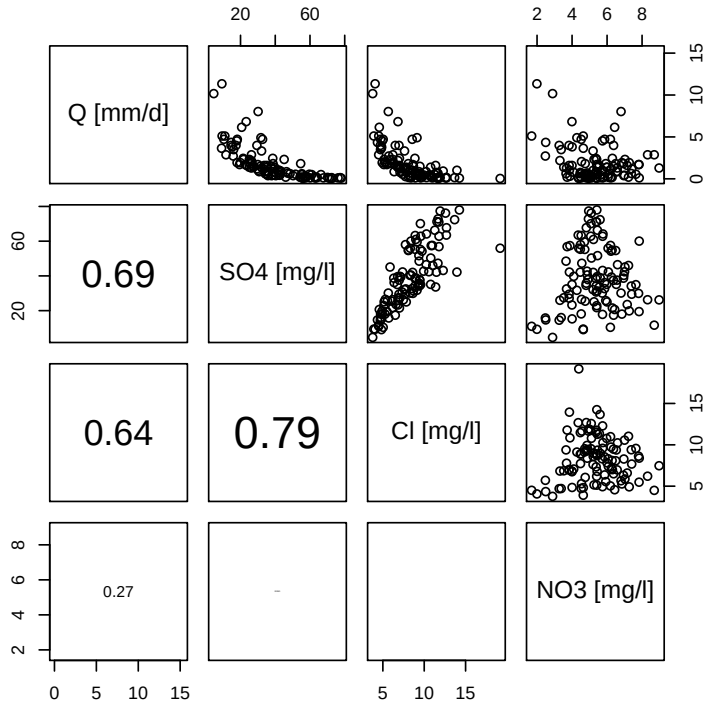

Figure 4.2: Correlation between discharge and solute concentrations (SO_4^{2-}, Cl^- and NO_3^-). The values represent the absolute correlation coefficient, with correlation strength given in font size.

days were set to zero. Chloride reached comparable values of 0.08 g/l as minimum, 2.04 mg/l as maximum and 0.89 mg/l as mean input concentration. As Figure 4.3 illustrates, the output concentration for both solutes was decidedly higher than the input concentration, although the difference between input and output is not quite as high for chloride as it is for sulfate. The output concentration for SO_4^{2-} ranged from 4.59 mg/l to 78.0 mg/l with a mean value of 38.83 mg/l. Chloride concentration in the spring was lower than sulfate, with an observed minimum of 3.78 mg/l, a maximum of 19.18 mg/l and mean value of 8.34 mg/l. Total mass flux out for sulfate was higher than input flux, while total mass flux out for chloride was lower than the input flux. Figure 4.3 depicts an increase in solute concentration during the dry summer months. High discharge on the other hand coincided with drops in solute concentration. Similar regimes can be seen for the other solutes measured in the spring, with the exception of NO_3^-, fluoride

(F^-) and potassium (K^+) (Figure 6.2). Nitrate peaks occurred at the beginning of the rainy season, after that, nitrate concentrations partly increased with discharge increase but partly decreased with discharge increase as well. Figure 4.2 supports the connection between discharge and concentration of the three solutes SO_4^{2-}, Cl^- and NO_3^-. While SO_4^{2-} and Cl^- show an exponential decrease in correlation with increasing discharge, the relation between NO_3^- and discharge is less distinct. Figure 4.2 further reveals a linear correlation between SO_4^{2-} and Cl^- with a correlation coefficient of 0.79.

4.3 rSAS

The solute concentration of SO_4^{2-} and Cl^- in the Rosario spring was predicted by separately applying the rSAS model for each solute. An optimised fit was reached by using the Nelder-Mead optimisation algorithm, which returned the parameters displayed in Table 4.1. It includes the fitted parameter $\log(\alpha)$ as well as its corresponding α. While background concentration, reaction rate and equilibrium concentration differ, due to the different solutes, the values for critical storage (dS_{crit}) are quite close. The critical storage for solutes is surpassed in the last year 2008/2009. The difference in the α and λ parameter is relatively high compared to the critical storage.

Table 4.1: Optimized rSAS parameter values of the best fit returned by the optimization algorithm (Nelder-Mead) for the two solutes.

	C_{back}	k1	C_{eq}	$\log(\alpha)$	α	λ	dS_{crit}
$\mathbf{SO_4^{2-}}$	38.65	0.00118	193.41	-0.0236	0.9767	-1.37	268.08
$\mathbf{Cl^-}$	28.15	0.00078	80.24	-2.2246	0.1081	-1.11	257.25

For each solute a different form of the age-ranked StorAge Selection function depending on storage and the optimised parameters was created. The gamma function distributions are plotted in Figure 4.4 for SO_4^{2-} and Figure 4.5 for Cl^-. For both solutes rSAS selects older water under low storage conditions, whereas under high storage conditions more young water is sampled. A notable difference between both gamma function distributions though is that the form of $\omega_Q(T)$ is more diverse for SO_4^{2-} as it varies between sampling more old water during low storage to sampling mainly young water under high storage conditions. The rSAS model for Cl^- samples more young water than the SO_4^{2-} model. For Cl^- at least 40 % of the water at any storage condition is young water of only a few

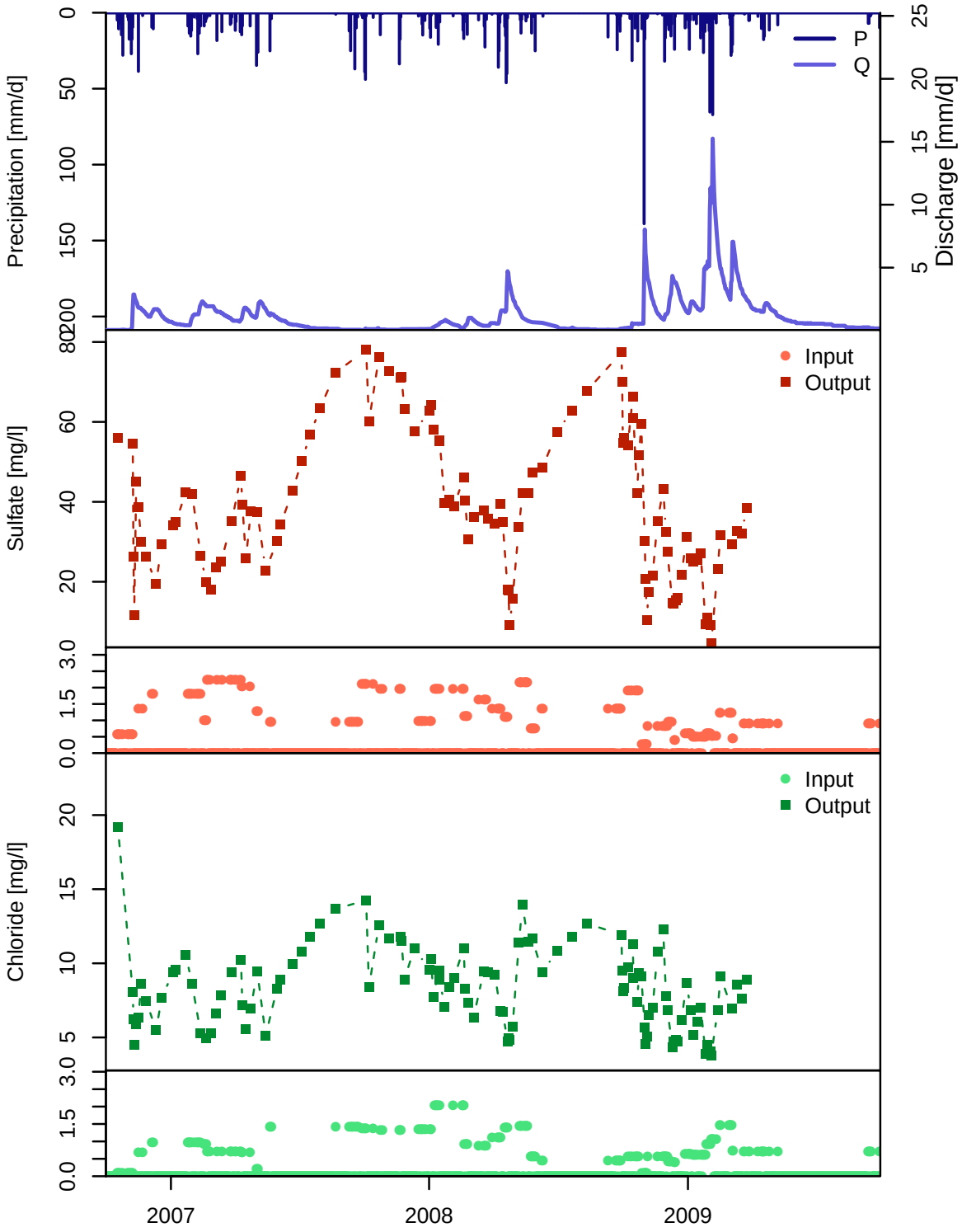

Figure 4.3: Time series of measured SO_4^{2-} and Cl^- concentrations in the input (precipitation bulk sample) and output (spring discharge), as well as time series of precipitation and discharge.

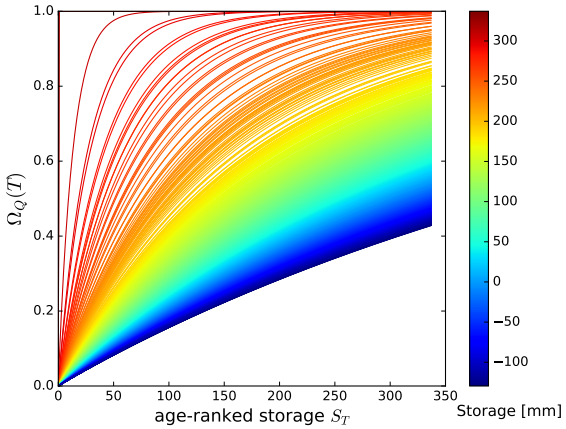

Figure 4.4: Cumulative rSAS function for SO_4^{2-} depending on storage volume.

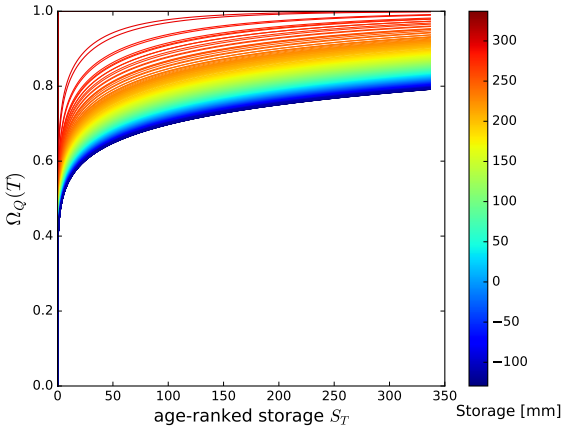

Figure 4.5: Cumulative rSAS function for Cl^- depending on storage volume.

days age. In contrast to that, water in the SO_4^{2-} model is always at least a few days old.

The cumulative transit time distributions for SO_4^{2-} (Figure 4.6) and Cl^- (Figure 4.7) are based on the rSAS function and have in general a similar form. The transit time distribution covered an increasing age during the course of the study, as the water aged through the storage. During 2006-2008 for both solutes mostly young water was sampled. The sampled water ages increased during 2007-2008. The wet year 2008-2009 showed a wider range of transit time distributions. During some days the discharge was sampled from the old storage, and then there were also some days where 80 % of the water sampled was younger than ∼100 days (SO_4^{2-}) or younger than ∼10 days (Cl^-).

Figure 4.8 displays the modelling results for SO_4^{2-}. The simulated concentration followed the general course of the measured concentrations of Rosario spring and reached a KGE of 0.80. The daily mean simulated output concentration is 51.85 mg/l, which is higher than the observed output concentration at 38.83 mg/l. Figure 4.8 displays the simulated concentrations in comparison to the observed concentrations. At the beginning of the modelling period in October 2006 the model first underestimated sulfate in the spring and then overestimated the concentrations until September 2007, with a few peak exceptions. The model did not follow the drops in concentration after major precipitation events. rSAS did follow the enrichment curve in the summer 2007, though it

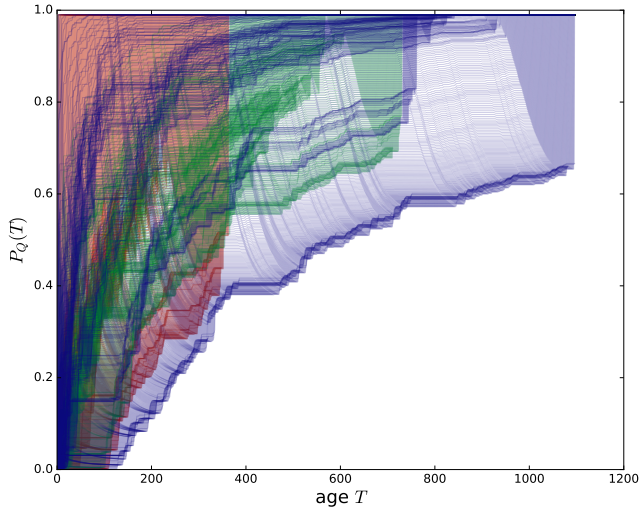

Figure 4.6: Cumulative transit time distributions for SO_4^{2-} for the different hydrologic years: 2006-2007 red, 2007-2008 green, 2008-2009 blue.

overestimated absolute values, as it started with higher concentrations from the spring. The first drop in concentration after both summers is predicted too early by the model. In fall 2007 the predicted concentrations fell below the observed concentrations until the beginning of 2008, when the simulated values where estimated too high again. The drop in concentration during the strongest precipitation event in the spring 2008 and during the major events in 2009 were predicted very closely by the model. The strong increase in concentration in 2009 cannot be evaluated due to missing observed data points.

The results for the rSAS simulation of the chloride concentration are displayed in Figure 4.9. The rSAS simulation for Cl^- reached a KGE of 0.71. The mean simulated concentration was 11.68 mg/l compared to a mean observed concentration of 8.34 mg/l in the spring. In contrast to the SO_4^{2-} simulation, the modelled chloride concentration started too high, but followed closely the drop in concentration with the onset of precipitation. For the rainy season 2006/2008 the model generally overestimated the Cl^- concentration but followed the increase in concentration during phases of decreasing discharge. It miscalculated the drops in concentration during that season, which were stronger than the model proposed. Similar to SO_4^{2-} the chloride concentration was overestimated during both summers with a drop in concentration earlier than the observed values suggest. The drop in concentration during the strongest precipitation event in the spring 2008 and during the major events in 2009 were predicted equally well as sulfate.

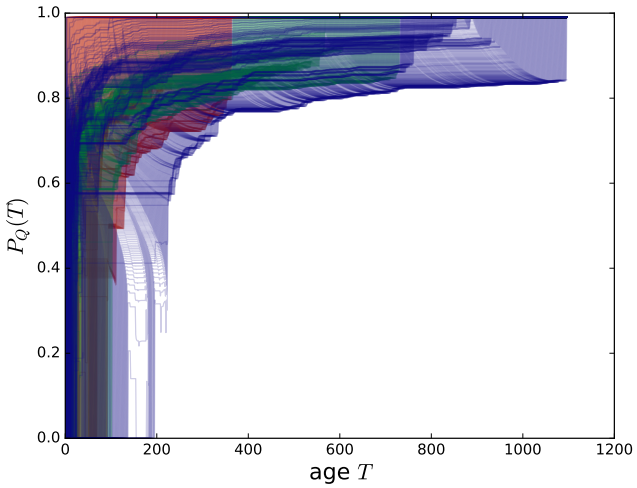

Figure 4.7: Cumulative transit time distributions for Cl^- for the different hydrologic years: 2006-2007 red, 2007-2008 green, 2008-2009 blue.

However, the chloride model underestimated the increase in concentration right after the events. Towards the end of the modelling period (30.08.2009) the model returns a peak of 50.45 mg/l.

For comparison a time-invariant model run with the parameters predicting sulfate concentration was done as well. The corresponding plot can be found in the Appendix (Figure 6.3). While the steady-state model did reach a KGE of 0.66, the simulated concentration followed the observed concentration during the dry season in 2008 and during fall/winter 2008/2009. rSAS predicted for the remaining time a straight, slightly increasing concentration of SO_4^{2-} in the spring.

4.4 Model evaluation

Based on the results of the optimization algorithm the limits for the parameter space of the Monte Carlo simulations were set to the values displayed in Table 3.1. The 30 000 Monte Carlo simulations concluded with the highest efficiency value of 0.79 and 0.70 for SO_4^{2-} and Cl^- respectively. This is close to the results returned by the optimization algorithm. As Figure 4.10 illustrates, for SO_4^{2-} the KS test determined a significant difference between the eCDF of the 500 behavioural runs compared to the eCDF of the non-behavioural runs for all parameters except λ. According to the HSY method the remaining parameters of the solute can be regarded as sensitive. To further differentiate

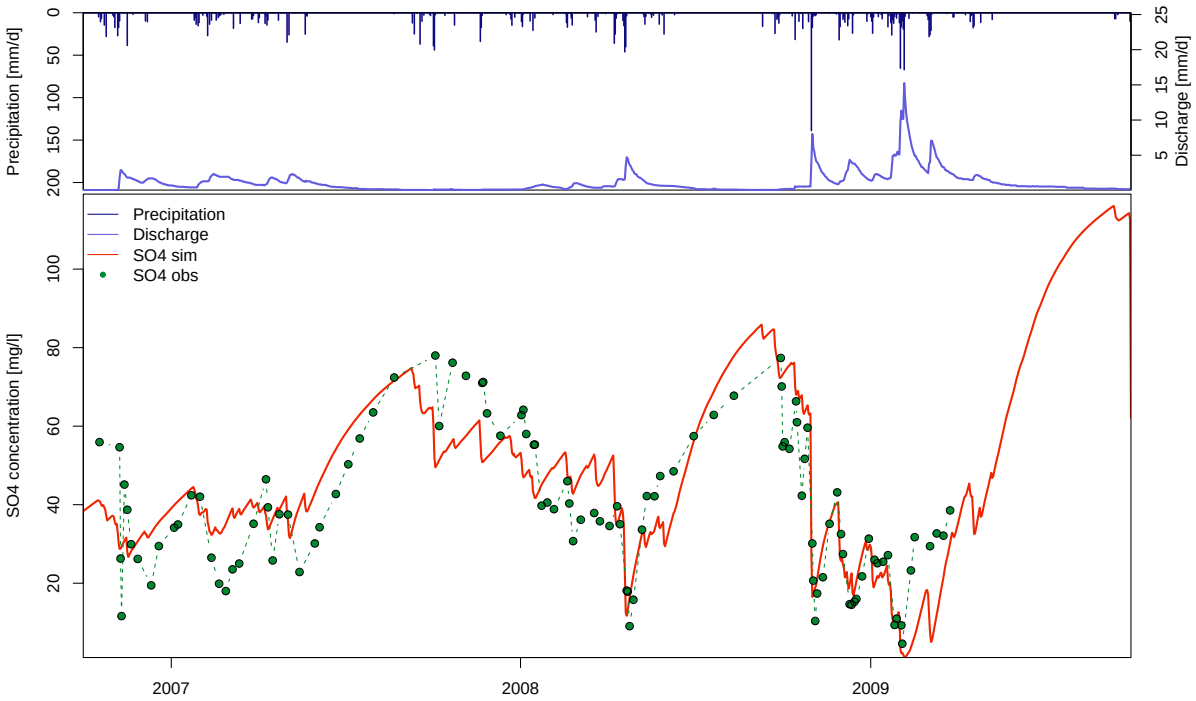

Figure 4.8: Time series of predicted sulfate concentration (SO4 sim) and observed sulfate concentration (SO4 obs) in the discharge calculated with a time-variant gamma function. Precipitation input and spring hydrograph time series for comparison.

between the strength of sensitivity the D statistic of the KS test is considered likewise depicted in Figure 4.10. While C_{back} has a low sensitivity and C_{eq} and $\log(\alpha)$ have a medium sensitivity, k1 and dS_{crit} are very sensitive parameters.

For Cl^- the HSY method determined different importance of the parameters as highlighted in Figure 4.11. All parameters are highly sensitive, if rSAS is applied to calculate the output concentration for chloride, except for λ, which has a medium sensitivity.

Applying GLUE to calculate the 95 % confidence interval revealed that the highest prediction uncertainty is during the dry summer period, when concentration increases. During the longer dry period in 2009 the prediction bounds spread farther than the two other summers. For both solutes not all observed concentrations fell within the confidence interval. As Figure 4.12 illustrates for SO_4^{2-} at the beginning of 2007 and

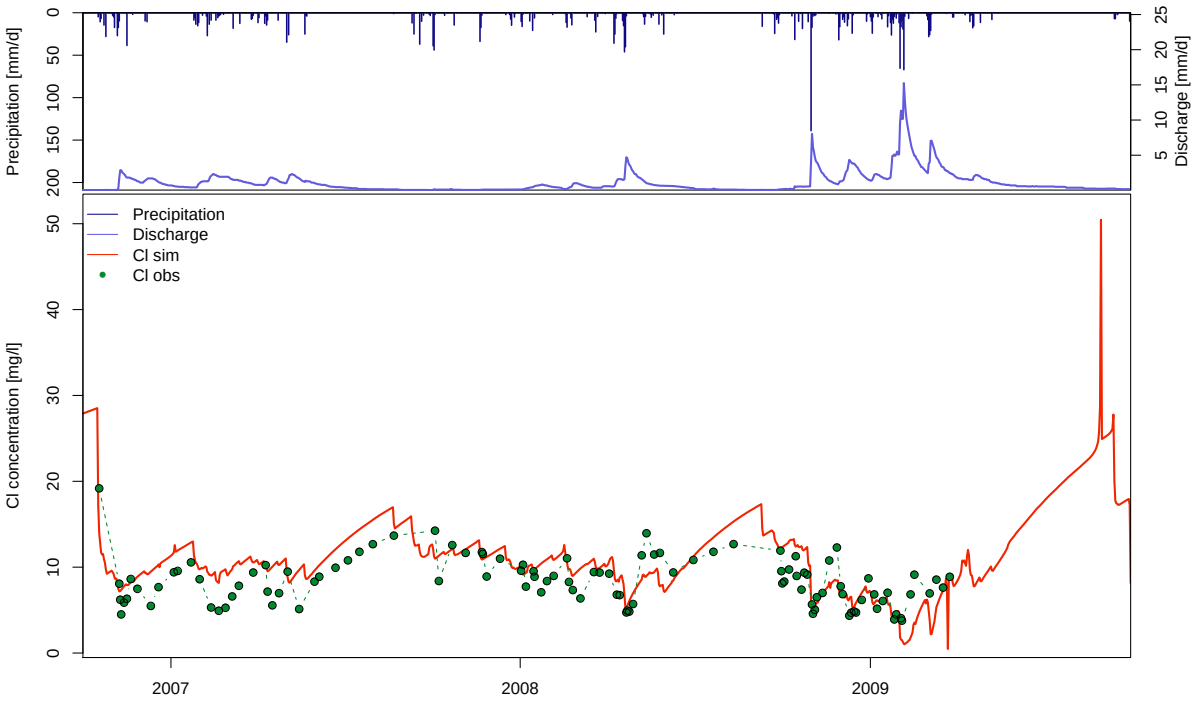

Figure 4.9: Time series of predicted chloride concentration (Cl sim) and observed chloride concentration (Cl obs) in the discharge calculated with a time-variant gamma function. Precipitation input and spring hydrograph time series for comparison.

2008, though not in 2009, rSAS overestimated SO_4^{2-} concentrations, with the observed concentrations in the lowest points of the curve lower than the 2.5 % quantile. The model further underestimated concentrations in the fall of 2007. A general agreement between most of the 500 behavioural models and the observed concentration were reached during the drop of SO_4^{2-} at the end of the wet season 2008 and during fall and winter 2008/2009. The predictive uncertainty and observed concentration for the modelling results of Cl^- are displayed in Figure 4.13. With few exceptions the observed concentration fell close to or within the confidence interval. Modelling uncertainty is high right at the beginning of the modelled time period but decreased with the start of the wet season 2006/2007, where only a few drops in concentration are underestimated by the model. Similar to

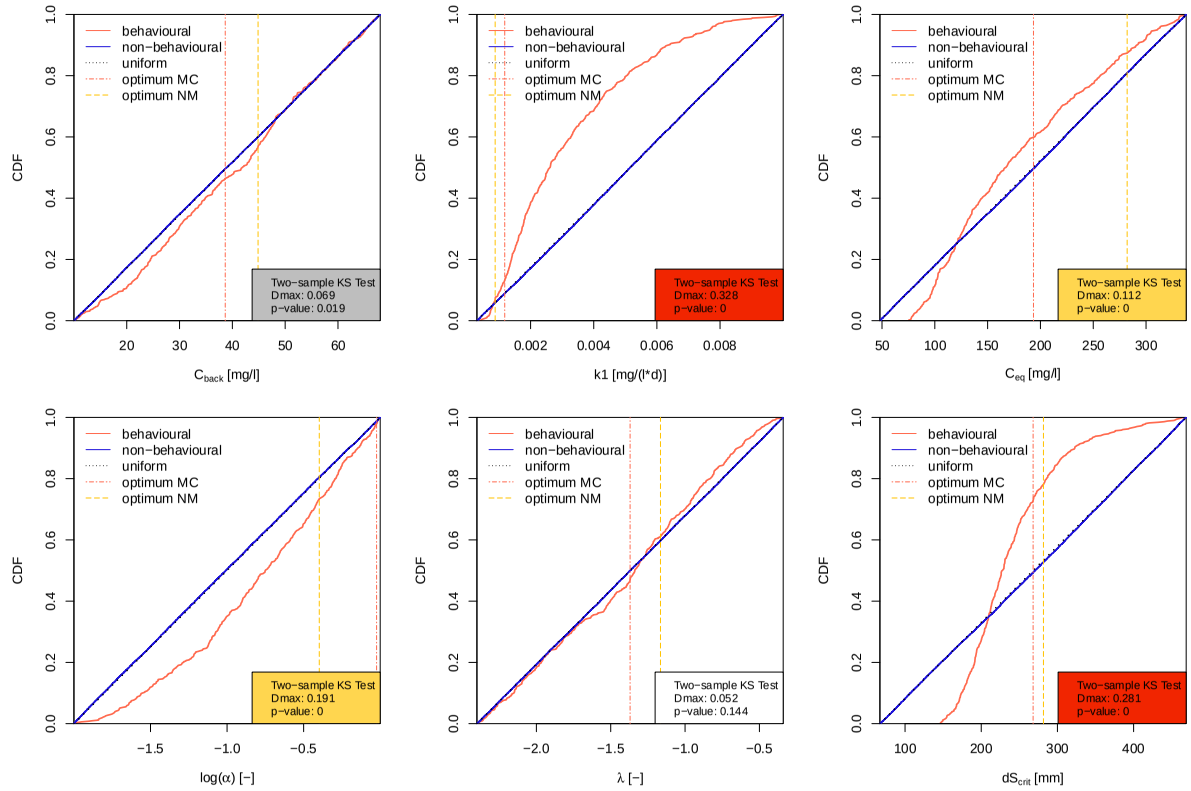

Figure 4.10: Results of the Hornberge-Spear-Young parameter sensitivity analysis for $SO_4{}^{2-}$: Comparison between the eCDF for the behavioural and non-behavioural Monte Carlo runs. Red box: high sensitivity, orange box: medium sensitivity, grey box: low sensitivity, white box: not sensitive. The dashed lines mark the parameter value of the Nelder-Mead algorithm (optimum NM) and of the Monte Carlo run with the highest efficiency (optimum MC).

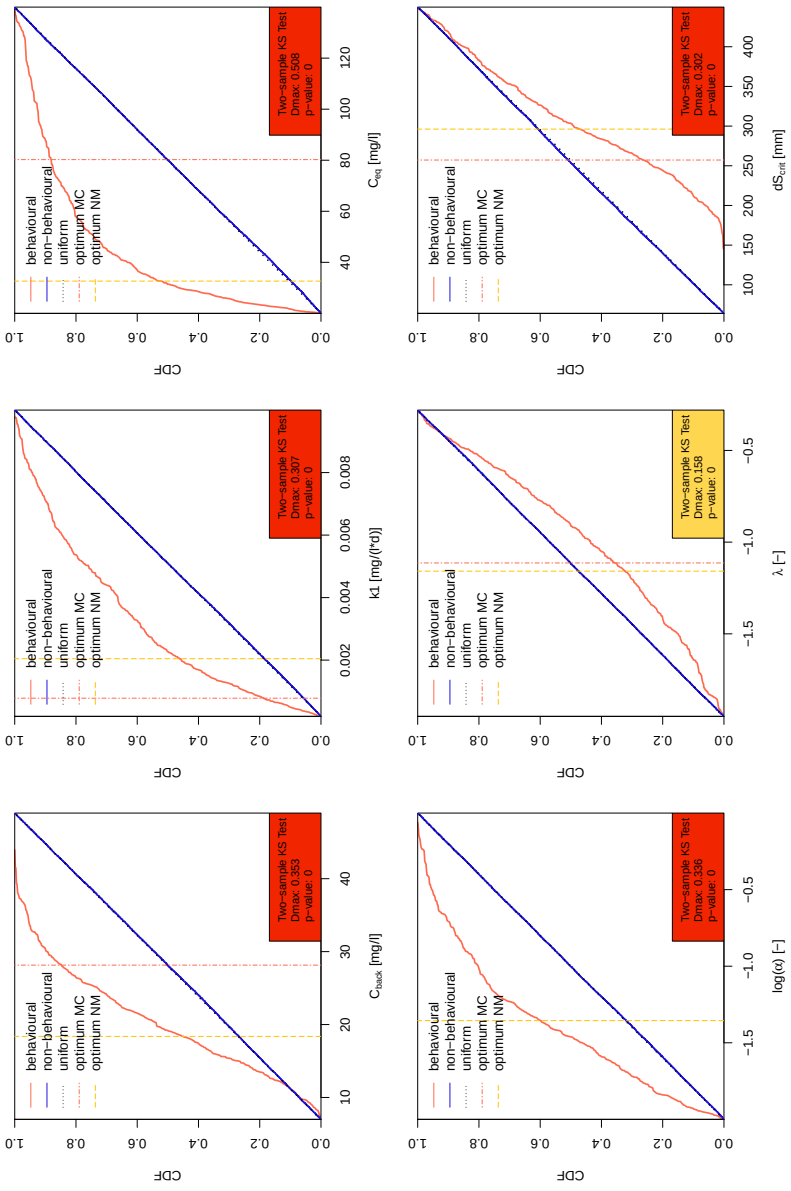

Figure 4.11: Results of the Hornberge-Spear-Young parameter sensitivity analysis for Cl^-: Comparison between the eCDF for the behavioural and non-behavioural Monte Carlo runs. Red box: high sensitivity, orange box: medium sensitivity, grey box: low sensitivity, white box: not sensitive. The dashed lines mark the parameter value of the Nelder-Mead algorithm (optimum NM) and of the Monte Carlo run with the highest efficiency (optimum MC).

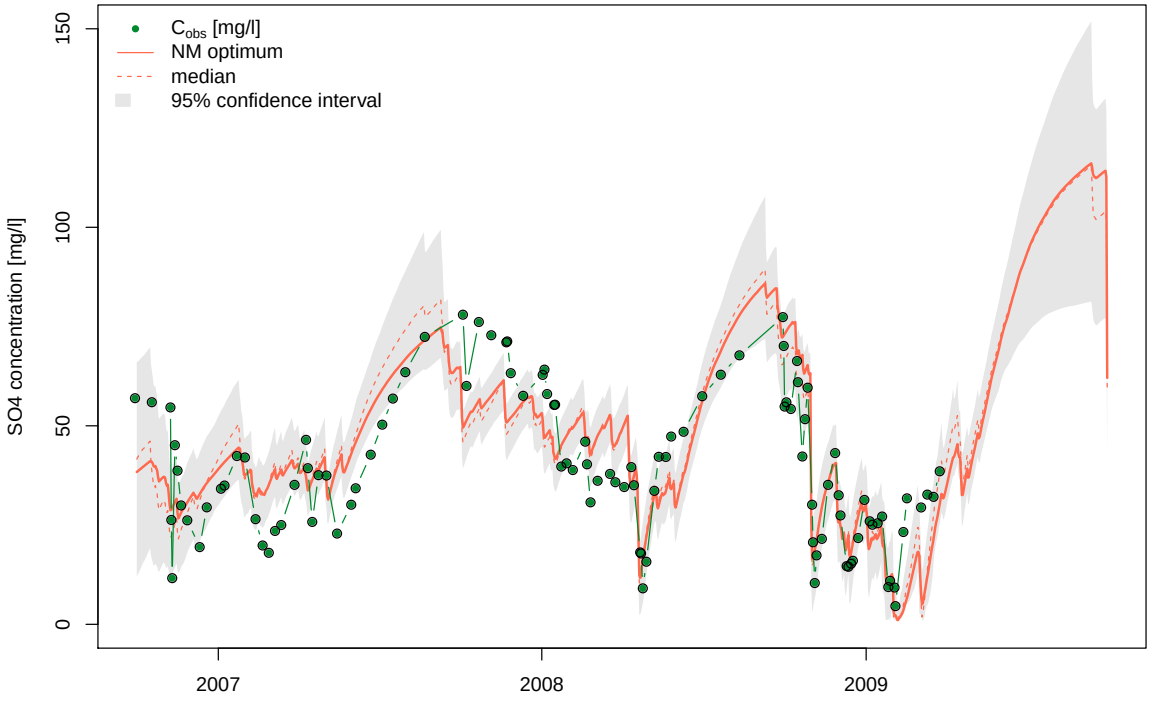

Figure 4.12: Results of GLUE for SO_4^{2-}: 95 % confidence interval and median of the behavioural Monte Carlo runs as well as the predicted concentration with the Nelder-Mead optimized parameters.

SO_4^{2-} the prediction uncertainty is low during the wet season 2008/2009, especially during the drops in concentration.

Based on the Kling-Gupta efficiency the rSAS model reached slightly better results than the semi-distributed VarKarst model. For SO_4^{2-} the KGE was 0.80 while VarKarst reached 0.69. The difference for Cl^- is similarly pronounced with a KGE of 0.71 for rSAS and 0.45 for VarKarst. A comparison between the graph of the simulated versus observed values of VarKarst and rSAS (Figure 4.14) revealed that rSAS predicted the SO_4^{2-} concentrations better for high concentrations. rSAS predictions were evenly scattered with some values overestimated and some underestimated. VarKarst underestimated more than overestimated. This effect is more pronounced for the predictions of Cl^-, where most values are underestimated by VarKarst as Figure 4.15 (a) illustrates. rSAS on the other hand tended to overestimate chloride concentrations, but again is mostly evenly scattered, as revealed by Figure 4.15 (b).

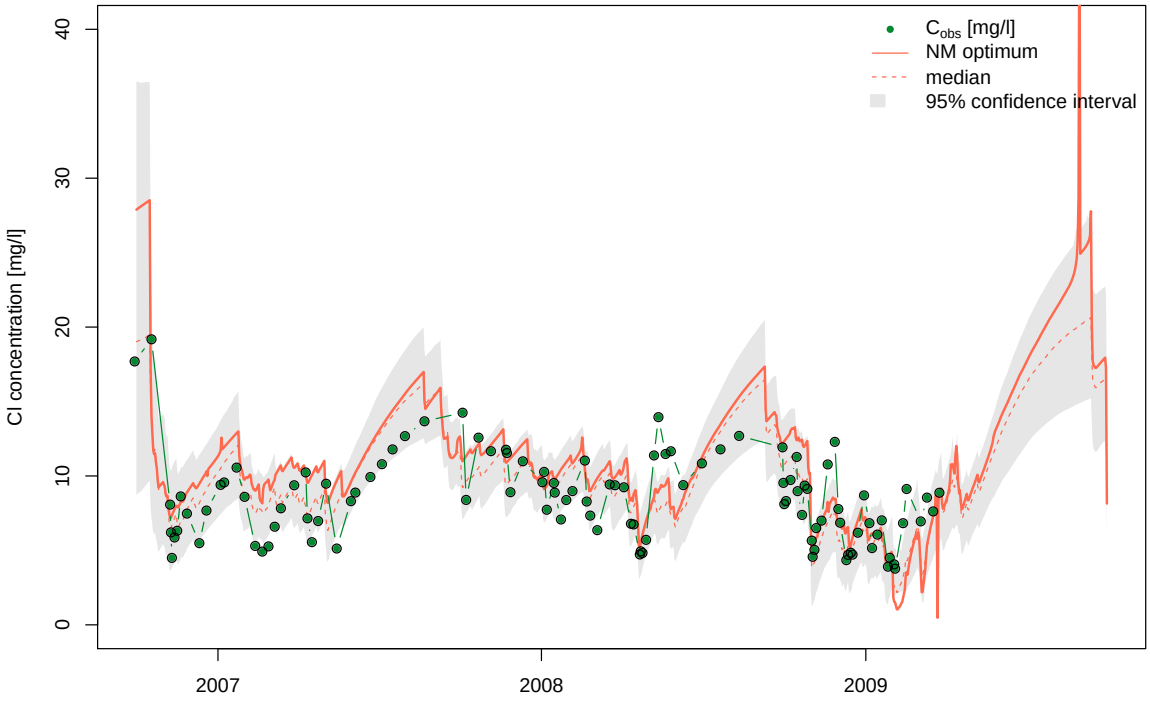

Figure 4.13: Results of GLUE for Cl^-: 95 % confidence interval and median of the behavioural Monte Carlo runs as well as the predicted concentration with the Nelder-Mead optimized parameters.

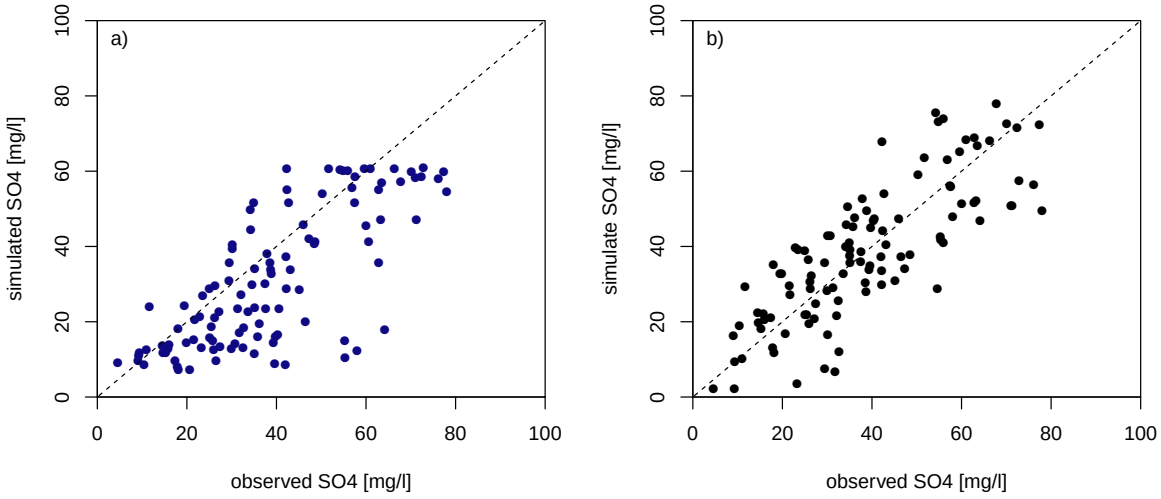

Figure 4.14: Observed versus simulated values with VarKarst (a) and rSAS (b) for SO_4^{2-}

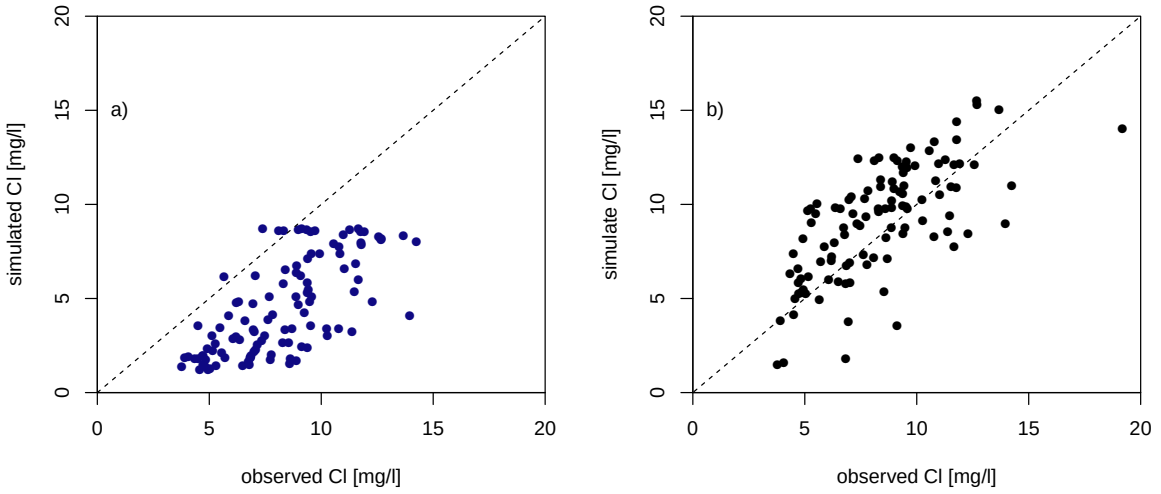

Figure 4.15: Observed versus simulated values with VarKarst (a) and rSAS (b) for Cl^-

5 Discussion

5.1 rSAS application and evaluation

The rSAS model has been applied to a karst catchment in southern Spain to test the hypothesis, that the new framework is able to model satisfactorily the solute transport in a complex flow system. The results which will be discussed in this section, allow the conclusion that the rSAS model can predict solute transport in this highly variable karst environment.

The Villanueva del Rosario catchment exhibits the typical landscape features, geology and flow regime of a karst catchment as described in several studies (Hartmann, Mudarra, et al., 2014; Mudarra and Andreo, 2011; Mudarra, Andreo, Barberá, et al., 2014). The recorded spring discharge during the study period reveals a corresponding flow behaviour, with a short time lag between precipitation and discharge and a strong increase in discharge after heavy precipitation events. This quick flow component can be explained by the existence of an underground conduit system. A long recession curve during the dry summer months on the other hand indicates the additional existence of a large matrix storage. Recharge values calculated for the Rosario catchment allowed Hartmann, Mudarra, et al., (2014) to reach similar conclusions, namely that the main source of spring water during drought periods was the karst matrix. The variable flow component and karstic nature of the system proved to be a suitable catchment to test the applicability of the rSAS framework. Hoewever, a certain degree of caution needs to be considered in regard to the input data for the model. Measured data retains a certain factor of inaccuracy that could impair reliability of the model. Precipitation is an especially error prone variable, where the error propagates into the storage calculation (Kirchner, 2009). The method to calculate storage itself relies on the accuracy of the input data as well as an assumed knowledge of all fluxes into and out of the system. The impact on the calculation with rSAS can nevertheless be deemed minor, as it does rely

on the relative storage and not the on absolute storage values.
A further data uncertainty affecting the modelling results is however the use of bulk samples to measure solute input. rSAS requires continuous input data, which in connection with a long measuring interval of two weeks or more means a possible error is introduced by interpolation. As the major part of the solutes is introduced into the system through geogenic dissolution, this inaccuracy is estimated low as well. An enrichment function is introduced into the model to cover the geogenic dissolution. Based on a concept by Benettin, Bailey, et al., (2015) it applied a first order reaction rate to simulate the dissolution of the minerals depending on contact time. Additional parameters which contribute to dissolution such as pH and temperature were neglected (Benettin, Bailey, et al., 2015). It can be discussed, if the reaction type is correct to model geogenic dissolution. However, the application of a full geochemical model would have gone beyond the scope of this thesis. The simpler solution of a first order reaction, as it was applied by Benettin, Bailey, et al., (2015) was therefore chosen to include geogenic dissolution. The application of an enrichment function is the reason, why NO_3^- was discarded as a potential tracer. It accumulates during the dry season and is flushed during the first precipitation events of the season. NO_3^- concentrations in the discharge depend to some extent on the time passed since the last precipitation event and not on the transit time, which could be seen in the correlation between discharge and NO_3^- concentration. The concentration is additionally to some extent influenced by anthropogenic input into the system. As there are some farming activities in the study area, the anthropogenic input could not be quantified, which makes it a less suitable tracer for this model. Chloride and Sulfate on the other hand, were chosen based on their widespread application as tracer in karst and other catchments.

Based on the achieved efficiency values and the comparison with the benchmark model VarKarst, it can be concluded that rSAS was able to predict solute transport in this karst catchment. This result supports the statement by Rinaldo et al., (2015) that SAS can potentially be applied to different flow systems. Especially the prediction of chloride proved to be better than the semi-distributed VarKarst model. Although the predicted solute concentration followed the general course of the observed concentration during the summer, rSAS predicted the drop in concentration too early in the summer 2007. Hartmann, Mudarra, et al., (2014) discovered, that the first rainfall of the season produces no or only limited amounts of recharge due to high evaporation values. The calculated actual evapotranspiration in this study were therefore potentially too low for the change

between dry season and wet season. This means that the storage mistakenly increased and influenced the shape of the selection function. Although most of the first rainfall of the season evaporated, it is assumed by rSAS to contribute to the discharge in terms of solute transport. As the observed values lay outside the confidence interval of the GLUE analysis during the change in season, it can be assumed to be a structural problem of the model in this area (Beven, 2012). The increase in uncertainty during the summer periods on the other hand is covered by the model. The enrichment function has the most impact during the summer month, where the most geogenic dissolution happens. Any faults with the simple first order reaction rate therefore contribute most during the summer month.

The accuracy of the rSAS prediction changed over the study period. While the changes in concentration were predicted well for both solutes for the wet year (2008/2009), the results for the first and second year were less compliant with the observed solute concentrations. On the start of the modelling period the water was sampled from the unknown storage with a set background concentration. It therefore contributed a large part to the discharge composition, although new input was quickly added. The start of the simulation is hence heavily influenced by the parameter C_{back}. The storage evolved during the study period, allowing a more defined storage to be sampled. This could explain, why the accuracy of rSAS improved for the last year. An additional factor contributing to this effect is the age of the water sampled. The form of the rSAS function and thus the percentages of young and old water it sampled depends on the storage. The reverse storage effect Harman, (2015) noticed for the Plynlimon watershed, where higher storage values are related to a higher percentage of event water, were observed for the Rosario catchment as well. A full storage was for both solutes associated with the sampling of younger water. As the storage during the wet year was higher than during the other two years, more young water with stored concentration informations was sampled and improved the accuracy of the discharge composition. The study period is too short to distinctively conclude if there is indeed a difference in accuracy between wet years and dry years or if the accuracy improved with each year analysed regardless of storage size. It is possible that a combination of both effects took place. It can therefore be argued, that a longer study period should improve modelling results, as well as allow a separate analysis of wet and dry years. McGuire and McDonnell, (2006) supports this reasoning, when he states that the accuracy of modelled transit times increases with data record

length. For reasons explained in the method section, a warmup would not have been suitable to improve modelling results.

The general form of the cumulative rSAS function $\omega_Q(T,t)$ differs between the two solutes. rSAS modelled with ${SO_4}^{2-}$ as tracer selected in average more water from the older part of the storage. The shape of the function was more influenced by the storage volume than for chloride, where the difference in shape between low storage conditions and high storage conditions was less pronounced. The average age of discharge modelled with ${SO_4}^{2-}$ would thus be older than for Cl^-. The difference of rSAS function and thus discharge age between the two solutes can be explained by the different locations of the solute sources within the aquifer. The triassic evaporites, which are the main source of sulfate are located deeper within the aquifer with some outcrops at the eastern border of the aquifer. To become enriched with sulfate the water travels through deeper layers and longer flowpaths. Water enriched with sulfate can therefore be assumed to be in average older than water with high chloride values, which are partly supplied by precipitation. As sulfate originates in the deeper layers it is furthermore continuously in contact with the saturated zone, with lower flow velocities and thus in average longer transit time in general and particularly during the summer months. This is especially visible for the last year of the study, when even the majority of the young water was at least 100 days old. Mudarra and Andreo, (2011) illustrate, that the deeper regions of the aquifer, where the evaporites are located, are saturated even at low storage conditions. Lopez-Chicano et al., (2001) noticed similar effects for evaporite layers in the Cabra-Alcaide massif, around 60 km north of the study area. The longer flow times through evaporites there were an effect of lower permeability. Marin et al., (2015) mapped the vulnerability of contamination in the Rosario catchment. One contributing reason for the lowest vulnerability class were amongst others the longer transit time. The areas assigned with this class correspond with areas of evaporite outcrops again at the eastern border of the catchment.

Chloride on the other hand has a less localized origin with sources throughout the depth of the aquifer. The two main sources of chloride in the rosario catchment are triassic rock and rainfall (Mudarra, Andreo, Marin, et al., 2014). In terms of modelling chloride can therefore be assumed to be a better tracer to represent overall catchment dynamics. The interpretation of the rSAS function indicates a large contribution of water aged 10 days or less during any storage condition. This is supported by the short

lag time between precipitation and discharge, which can be contributed to conduit flow. The findings correlate with the results by Mudarra and Andreo, (2011), who determined high flow velocities and short transit times in the Rosario catchment.

The difference between the two solutes is equally visible in the values and sensitivity of the parameters. Although SO_4^{2-} input is dependent on the enrichment function, only the reaction rate parameter is assessed as highly sensitive. The equilibrium concentration seems to be less relevant for the modelling output. Both parameters could not be confirmed by literature values. Gypsum has a equilibrium concentration of 2400 mg/l (Gutiérrez et al., 2008), which is several magnitudes higher than what was found as optimized parameter value for rSAS. The approach by Benettin, Bailey, et al., (2015) to assume equilibrium concentration during low flow conditions, instead of reaching the value through calibration, was not applicable for both solutes, as equilibrium concentration was never reached in the discharge. The dissolution rate could not be compared to literature values. Previous studies state the dissolution rate in mm of disolved gypsum per year in stead of mg/(l*d) (Klimchouk et al., 1996). As there is no information about the absolute amount of gypsum rock in the study area, the units are non transferable. The enrichment function parameter for chloride on the other hand are all highly sensitive. Although halite has a higher solubility than gypsum, the reaction rate parameter is still lower. This can be explained by the fact, that a major part of the chloride enters the system via precipitation and does not need to be simulated by the enrichment function. It seems for both solutes that the parameter of the enrichment function are dependent on the absolute amount of rock, with which they come in contact. As this can not be quantified, it can be established that the enrichment function parameter values itself contribute no information about the aquifer. However, since the reaction rate of chloride is very low, it can be argued, that chloride could potentially be modelled without the enrichment function. It would further support the assumption, that chloride as a tracer is a better suited to model catchment dynamics with rSAS. A potential solution to not lose the information supplied by the spatial distribution of SO_4^{2-}, could be to combine the rSAS optimized parameter α, λ and dS_{crit} for chloride and fit new parameter for the enrichment function of SO_4^{2-}.
The rSAS parameter for chloride transport had high or medium sensitivity. The α parameter controlled the shape of the rSAS function and thus the proportion of young water that was sampled from the storage. With a large α more old water is sampled,

with a small α more water from the younger part of the storage is drawn. The α value of the non-karstic Plynlimon watershed in Wales is with 0.69 in the middle between the values for the two tracer (Harman, 2015). It is reasonable, that a karst catchment with short flow times had a higher percentage event water in the discharge and thus a smaller α value. Hrachowitz et al., (2010) confirms, that the α parameter of the gamma function to describe transit time distributions is dependent on catchment characteristics. The application of rSAS to additional catchments in the future might contribute more information as to how the parameter is connected to catchment characteristics. The critical storage parameter is related to catchment flow systems. The closer the storage is to the critical storage, the more event water contributes to discharge. The one time storage values in the Rosario catchment crossed the critical storage was during a heavy precipitation event with the highest discharge of the three years. The reaction of natural and artificial tracer during this event lead Mudarra and Andreo, (2011) to the conclusion, that the Rosario catchment had a limited storage capacity, with fast reaction times. dS_{crit} values found by Harman, (2015) were considerable lower at 48 mm, but they were combined with considerably lower λ values as well of -103 mm and are thus difficult to compare. λ itself is not connected to a physical interpretation, but is a fitting parameter according to Harman, (2015).

The comparison between rSAS and the benchmark model proved that rSAS was able to reach and surpass the benchmark model VarKarst in regard to its ability to predict solute concentration. While SO_4^{2-} concentration were predicted equally well, the difference is noticeable in the prediction of chloride concentration, where rSAS reached higher efficiency values. Although rSAS might perform better at predicting solute transport, there are two advantages to VarKarst. It can be used to calculate the temporal variability of recharge and it can be combined with a distributed model to cover the spatial variability of recharge as well (Hartmann, Mudarra, et al., 2014). rSAS as a new framework has yet to be further developed to expand its application beyond solute and transit time modelling.

5.2 rSAS model structure

One question to be discussed was the model type of the rSAS concept. The assumption of an age-ranked storage in the model, which provides information about the transit

time distributions of discharge, allows the conclusion, that rSAS is more than a transfer function between input and output and can thus be deemed a grey-box model. If a model predicts solute concentrations accurately, it can be argued that the transit time distributions were simulated correctly. Hence it might be deduced that the model is an valid representation of catchment processes (McDonnell et al., 2010). As the previous section proved, rSAS was able to predict solute transport , it thus assumedly predicts transit times correctly as well, if the tracer source is taken into account. However, the comparison between the two different solute tracer indicates that a certain knowledge about the geology of the catchment is necessary for a valid interpretation. The alternative would be to use, if available, isotope data, which are known to have an even input throughout the catchment. Nevertheless, a global tracer in the rSAS model, returns not only information about the output, but about the age composition of the discharge as well. With the information about transit times it is for example possible to model the behaviour of a contaminant within the storage.

The use of a state variable such as storage connects transit time predictions to the physical environment, thus making rSAS more than a black-box model. Mudarra and Andreo, (2011) illustrated that storage volume and flow path variability are directly related in the Rosario catchment. They established that under high water conditions more karst conduits are active, which explains short transit times. This is mirrored by the rSAS model, where more young water in the storage is sampled during high storage conditions. This feature is controlled by the parameter critical storage (dS_{crit}). The shape parameter α is an additonal parameter that is potentially connected to physical catchment characteristics as suggested by Harman, (2015) and Hrachowitz et al., (2010). However, the experience with rSAS at this point is to limited to interpret the parameter value.

6 Synthesis

6.1 Conclusion

The newly developed rSAS framework was applied to the Villanueva del Rosario catchment in northern Spain to test the performance of the model in a karst catchment for the first time. It was applied to predict the discharge concentration of two solutes: sulfate and chloride. The solutes enter the catchment through precipitation as well as geogenic dissolution. An enrichment function was included in the model to calculate geogenic tracer input. It was based on the concept that solute concentration in the spring is dependent on the contact time between water and mineral, which are gpysum and halite in this study. A first order reaction based on equilibrium concentration, reaction rate and contact time, which is taken from the rSAS calculation, was used to calculate the enrichment of the water with solutes. The new rSAS framework applies the concept of an age-ranked storage, from which discharge is chosen according to a selection function. For this study a two parameter gamma function with a storage dependent scale parameter was chosen as rSAS function. The time-variance of transit time distributions under different states of catchment wetness was thus taken into account. The model was able to predict solute concentration in the discharge with an efficiency of 0.80 for SO_4^{2-} and 0.71 for Cl^-. With these results it reached and surpassed the benchmark model VarKarst. However, a closer analysis of the results returned by the application to sulfate revealed the problem that SO_4^{2-} as a tracer provided information about deeper aquifer layers, where the gypsum is located and not about the whole catchment area. Chloride on the other hand, was determined to be a good representative of catchment dynamics. The transit times returned by the model corresponded to the results of Mudarra and Andreo, (2011), who performed extensive natural and artificial tracer experiments in the Rosario catchment. The hypothesis that rSAS is able to model solute transport in a karst catchment can thus be confirmed. Additionally, it was discussed if rSAS can be

classified as a black-box or a grey-box model. As the physical properties of the catchment were included into the model by using storage as a state-variable, it was decided, that rSAS should be considered a grey-box model. This study expanded the knowledge about StorAge Selection functions and about rSAS in particular. It has now been established that rSAS can potentially be applied in a system with variable flow characteristics such as karst.

6.2 Outlook

As rSAS is a new framework it has not been widely test yet. While this study contributes to expand the experience with rSAS, it also leaves room for improvement. A major impediment on the significance of the results is the short study period. The accuracy of the parametrized StorAge selection function could potentially improve if a longer data record was available. For a future application of the rSAS framework at catchment level it is therefore recommended to use a longer data record, which ideally consists of both solute and isotope data. The application to a different karst system would additionally assess if the experience with this study is transferable to other karst systems. The internal difference between various karst systems commonly results in a difficulty to transfer modelling approaches. rSAS might be an exception for this as the assumed general applicability of SAS functions allows to reason that rSAS will perform well in other systems. The application to additional catchments, karst and non-karst, could furthermore support the analysis of a potential connection between catchment characteristics and rSAS parameter values. Finally, rSAS could be tested to actually model contaminant transport. If the behaviour of the contaminant in the aquifer is known, transit time distributions can be used to predict the release of the contaminant into the catchment outlet. A model that could more easily supply this information might contribute to the safety of drinking water supplies.

Bibliography

Amin, Isam E. and M. E. Campana (1996). "A general lumped parameter model for the interpretation of tracer data and transit time calculation in hydrologic systems". In: *Journal of Hydrology* 179.1-4, pp. 1–21. ISSN: 0022-1694. DOI: \url{10.1016/0022-1694(95)02880-3}.

Andreo, B. et al. (2008). "Methodology for groundwater recharge assessment in carbonate aquifers: Application to pilot sites in southern Spain". In: *Hydrogeology Journal* 16.5, pp. 911–925. ISSN: 1431-2174. DOI: \url{10.1007/s10040-008-0274-5}.

Bakalowicz, Michel (2005). "Karst groundwater: A challenge for new resources". In: *Hydrogeology Journal* 13.1, pp. 148–160. ISSN: 1431-2174. DOI: \url{10.1007/s10040-004-0402-9}.

Bakalowicz, Michel and A. Mangin (1980). "L'aquifere karstique. Sa definition, ses characteristiques et son identification." In: *Memoires de la Societe Geologique de France* 11, pp. 71–79.

Batiot, Christelle, Christophe Emblanch, and Bernard Blavoux (2003). "Carbone organique total (COT) et magnésium (Mg 2+): deux traceurs complémentaires du temps de séjour dans l'aquifère karstique". In: *Comptes Rendus Geoscience* 335.2, pp. 205–214.

Batiot, Christelle, Cristina Liñán, et al. (2003). "Use of Total Organic Carbon (TOC) as tracer of diffuse infiltration in a dolomitic karstic system: The Nerja Cave (Andalusia, southern Spain)". In: *Geophysical Research Letters* 30.22. ISSN: 1944-8007. DOI: \url{10.1029/2003GL018546}. URL: %5Curl%7Bhttp://onlinelibrary.wiley.com/doi/10.1029/2003GL018546/full%7D.

Beck, M. B. (1987). "Water quality modeling: A review of the analysis of uncertainty". In: *Water Resources Research* 23.8, pp. 1393–1442. ISSN: 00431397. DOI: \url{10.1029/WR023i008p01393}.

Benettin, Paolo, Scott W. Bailey, et al. (2015). "Linking water age and solute dynamics in streamflow at the Hubbard Brook Experimental Forest, NH, USA". In: *Water Resources Research* 51.11, pp. 9256–9272. ISSN: 00431397. DOI: \url{10.1002/2015WR017552}.

Benettin, Paolo, James W. Kirchner, et al. (2015). "Modeling chloride transport using travel time distributions at Plynlimon, Wales". In: *Water Resources Research* 51.5, pp. 3259–3276. ISSN: 00431397. DOI: \url{10.1002/2014WR016600}.

Beven, K. (2012). *Rainfall-runoff modelling: The primer*. 2nd ed. Hoboken: Wiley. ISBN: 9780470714591.

Beven, K. and Andrew Binley (1992). "The future of distributed models: Model calibration and uncertainty prediction". In: *Hydrological Processes* 6.3, pp. 279–298. ISSN: 08856087. DOI: \url{10.1002/hyp.3360060305}.

Birkel, Christian et al. (2012). "High-frequency storm event isotope sampling reveals time-variant transit time distributions and influence of diurnal cycles". In: *Hydrological Processes* 26.2, pp. 308–316. ISSN: 08856087. DOI: \url{10.1002/hyp.8210}.

Bolin, Bert and H. Rodhe (1973). "A note on the concepts of age distribution and transit time in natural reservoirs". In: *Tellus* 25.1, pp. 58–62. ISSN: 00402826. DOI: \url{10.1111/j.2153-3490.1973.tb01594.x}.

Botter, G., E. Bertuzzo, and A. Rinaldo (2010). "Transport in the hydrologic response: Travel time distributions, soil moisture dynamics, and the old water paradox". In: *Water Resources Research* 46.3, n/a–n/a. ISSN: 00431397. DOI: \url{10.1029/2009WR008371}.

— (2011). "Catchment residence and travel time distributions: The master equation". In: *Geophysical Research Letters* 38.11, n/a–n/a. ISSN: 00948276. DOI: \url{10.1029/2011GL047666}.

Butscher, C. and P. Huggenberger (2009). "Modeling the Temporal Variability of Karst Groundwater Vulnerability, with Implications for Climate Change". In: *Environmental Science & Technology* 43.6, pp. 1665–1669. ISSN: 0013-936X. DOI: \url{10.1021/es801613g}.

Christensen, J.H. et al. (2007). "Regional Climate Projections". In: *The physical science basis*. Ed. by IPCC. Vol. contribution of Working Group ... to the fourth assessment report of the Intergovernmental Panel on Climate Change ; Working Group 1. Climate change 2007. Cambridge [u.a.]: Cambridge Univ. Press. ISBN: 0521880092.

COST 65 (1995). *Hydrogeological aspects of groundwater protection in karstic areas: COST action 65*. Vol. 16526. EUR. Luxembourg: Office for Official Publications of the European Communities. ISBN: 92-827-4679-8.

Danckwerts, P. V. (1953). "Continuous flow systems: Distribution of residence times". In: *Chemical Engineering Science*, pp. 1–13. ISSN: 00092509.

Debeglia, N., A. Bitri, and P. Thierry (2006). "Karst investigations using microgravity and MASW; Application to Orléans, France". In: *Near Surface Geophysics* 4.13. ISSN: 18730604. DOI: \url{10.3997/1873-0604.2005046}.

Deng, Ju-Long (1982). "Control problems of grey systems". In: *Systems & Control Letters* 1.5, pp. 288–294. ISSN: 01676911. DOI: \url{10.1016/S0167-6911(82)80025-X}.

Denić-Jukić, Vesna and Damir Jukić (2003). "Composite transfer functions for karst aquifers". In: *Journal of Hydrology* 274.1, pp. 80–94. ISSN: 0022-1694.

Einsiedl, F. (2005). "Flow system dynamics and water storage of a fissured-porous karst aquifer characterized by artificial and environmental tracers". In: *Journal of Hydrology* 312.1-4, pp. 312–321. ISSN: 0022-1694. DOI: \url{10.1016/j.jhydrol.2005.03.031}.

Etcheverry, David and Pierre Perrochet (2000). "Direct simulation of groundwater transit-time distributions using the reservoir theory". In: *Hydrogeology journal* 8.2, pp. 200–208. ISSN: 1431-2174. DOI: \url{10.1007/s100400050006}.

Field, Malcolm S. (1997). In: *Environmental Monitoring and Assessment* 47.1, pp. 23–37. ISSN: 01676369. DOI: \url{10.1023/A:1005782102565}.

Ford, D. C. and P.W. Williams (2007). *Karst hydrogeology and geomorphology*. [Rev. ed.] Chichester, England and Hoboken, NJ: John Wiley & Sons. ISBN: 978-0-470-84996-5. DOI: \url{10.1002/9781118684986}. URL: %5Curl%7Bhttp://site.ebrary.com/lib/alltitles/docDetail.action?docID=10295774%7D.

Ghasemizadeh, Reza et al. (2012). "Review: Groundwater flow and transport modeling of karst aquifers, with particular reference to the North Coast Limestone aquifer system of Puerto Rico". In: *Hydrogeology journal* 20.8, pp. 1441–1461. ISSN: 1431-2174. DOI: \url{10.1007/s10040-012-0897-4}.

Goldscheider, N. and David Drew (2007). *Methods in Karst Hydrogeology: IAH: International Contributions to Hydrogeology, 26*. CRC Press. ISBN: 0203934628.

Goldscheider, N. et al. (2008). "Tracer tests in karst hydrogeology and speleology". In: *International Journal of Speleology* 37.1, pp. 27–40. ISSN: 0392-6672. DOI: \url{10.5038/1827-806X.37.1.3}.

Gupta, Hoshin V. et al. (2009). "Decomposition of the mean squared error and NSE performance criteria: Implications for improving hydrological modelling". In: *Journal of Hydrology* 377.1-2, pp. 80–91. ISSN: 0022-1694. DOI: \url{10.1016/j.jhydrol.2009.08.003}.

Gutiérrez, F. et al. (2008). "Geological and environmental implications of the evaporite karst in Spain". In: *Environmental Geology* 53.5, pp. 951–965. ISSN: 0943-0105. DOI: \url{10.1007/s00254-007-0721-y}.

Hao, Yonghong et al. (2006). "A gray system model for studying the response to climatic change: The Liulin karst springs, China". In: *Journal of Hydrology* 328.3-4, pp. 668–676. ISSN: 0022-1694. DOI: \url{10.1016/j.jhydrol.2006.01.022}.

Harman, C. J. (2015). "Time–variable transit time distributions and transport: Theory and application to storage–dependent transport of chloride in a watershed". In: *Water Resources Research* 51.1, pp. 1–30. ISSN: 1944-7973. URL: %5Curl%7Bhttp://onlinelibrary.wiley.com/doi/10.1002/2014WR015707/full%7D.

— (2016). *rsas library 0.1.1: Branch: rsas-fort*. URL: %5Curl%7Bhttps://github.com/charman2/rsas/tree/fort%7D (visited on 12/07/2016).

Harman, C. J., A. S. Ward, and A. Ball (2016). "How does reach-scale stream-hyporheic transport vary with discharge? Insights from rSAS analysis of sequential tracer injections in a headwater mountain stream". In: *Water Resources Research*. ISSN: 00431397. DOI: \url{10.1002/2016WR018832}.

Hartmann, A., J. A. Barberá, et al. (2013). "Progress in the hydrologic simulation of time variant recharge areas of karst systems – Exemplified at a karst spring in Southern Spain". In: *Advances in Water Resources* 54, pp. 149–160. ISSN: 03091708. DOI: \url{10.1016/j.advwatres.2013.01.010}.

Hartmann, A., N. Goldscheider, et al. (2014). "Karst water resources in a changing world: Review of hydrological modeling approaches". In: *Reviews of Geophysics* 52.3, pp. 218–242. ISSN: 87551209. DOI: \url{10.1002/2013RG000443}.

Hartmann, A., M. Mudarra, et al. (2014). "Modeling spatiotemporal impacts of hydroclimatic extremes on groundwater recharge at a Mediterranean karst aquifer". In: *Water Resources Research* 50.8, pp. 6507–6521. ISSN: 00431397. DOI: \url{10.1002/2014WR015685}.

Hartmann, A., M. Weiler, et al. (2013). "Process-based karst modelling to relate hydrodynamic and hydrochemical characteristics to system properties". In: *Hydrology and Earth System Sciences* 17.8, pp. 3305–3321. ISSN: 1607-7938. DOI: \url{10.5194/hess-17-3305-2013}.

Hartmann, A. et al. (2012). "Identification of a karst system's intrinsic hydrodynamic parameters: Upscaling from single springs to the whole aquifer". In: *Environmental Earth Sciences* 65.8, pp. 2377–2389. ISSN: 1866-6299. DOI: \url{10.1007/s12665-011-1033-9}.

Heidbüchel, Ingo, P. Troch, and S. Lyon (2013). "Separating physical and meteorological controls of variable transit times in zero-order catchments". In: *Water Resources Research* 49.11, pp. 7644–7657. ISSN: 00431397. DOI: \url{10.1002/2012WR013149}.

Hrachowitz, M. et al. (2010). "Gamma distribution models for transit time estimation in catchments: Physical interpretation of parameters and implications for time-variant transit time assessment". In: *Water Resources Research* 46.10, n/a–n/a. ISSN: 00431397. DOI: \url{10.1029/2010WR009148}.

Hrachowitz, M. et al. (2013). "What can flux tracking teach us about water age distribution patterns and their temporal dynamics?" In: *Hydrology and Earth System Sciences* 17.2, pp. 533–564. ISSN: 1607-7938. DOI: \url{10.5194/hess-17-533-2013}.

Jacob, Thomas et al. (2008). "Absolute gravity monitoring of water storage variation in a karst aquifer on the larzac plateau (Southern France)". In: *Journal of Hydrology* 359.1-2, pp. 105–117. ISSN: 0022-1694. DOI: \url{10.1016/j.jhydrol.2008.06.020}.

Jacob, Thomas et al. (2010). "Time-lapse microgravity surveys reveal water storage heterogeneity of a karst aquifer". In: *Journal of Geophysical Research* 115.B6. ISSN: 0148-0227. DOI: \url{10.1029/2009JB006616}.

Jukić, Damir and Vesna Denić-Jukić (2006). "Nonlinear kernel functions for karst aquifers". In: *Journal of Hydrology* 328.1, pp. 360–374. ISSN: 0022-1694.

— (2009). "Groundwater balance estimation in karst by using a conceptual rainfall–runoff model". In: *Journal of Hydrology* 373.3-4, pp. 302–315. ISSN: 0022-1694. DOI: \url{10.1016/j.jhydrol.2009.04.035}.

Kim, Minseok et al. (2016). "Transit time distributions and StorAge Selection functions in a sloping soil lysimeter with time-varying flow paths: Direct observation of internal and external transport variability". In: *Water Resources Research*. ISSN: 00431397. DOI: \url{10.1002/2016WR018620}.

Kiraly, L. (1975). “Rapport sur l’état actuel des connaissances dans le domaine des caractères physiques des roches karstiques”. In: *Hydrogeology of karstic terrains*. Ed. by A. Burger and Louis Dubertret. Vol. v. 1. International contributions to hydrogeology. Hannover, West-Germany: Heise, pp. 53–67. ISBN: 9783922705055.

— (1998). “Modelling karst aquifers by the combined discrete channel and continuum approach”. In: *Bulletin d’Hydrogéologie* 16, pp. 77–98.

Kirchner, James W. (2009). “Catchments as simple dynamical systems: Catchment characterization, rainfall-runoff modeling, and doing hydrology backward”. In: *Water Resources Research* 45.2, n/a–n/a. ISSN: 00431397. DOI: \url{10.1029/2008WR006912}.

Kirchner, James W., Xiahong Feng, and C. Neal (2000). “Fractal stream chemistry and its implications for contaminant transport in catchments”. In: *Nature* 403.6769, pp. 524–527. ISSN: 0028-0836. DOI: \url{10.1038/35000537}.

— (2001). “Catchment-scale advection and dispersion as a mechanism for fractal scaling in stream tracer concentrations”. In: *Journal of Hydrology* 254.1-4, pp. 82–101. ISSN: 0022-1694. DOI: \url{10.1016/S0022-1694(01)00487-5}.

Kirn, L. et al. (2016). “Improved Assessment of Groundwater Recharge in a Mediterranean Karst Region - Andalusia, Spain: Unpublished results”. Unpublished results.

Klaus, J. and J. J. McDonnell (2013). “Hydrograph separation using stable isotopes: Review and evaluation”. In: *Journal of Hydrology* 505, pp. 47–64. ISSN: 0022-1694. DOI: \url{10.1016/j.jhydrol.2013.09.006}.

Klimchouk, A. B. and S. D. Aksem (2005). “Hydrochemistry and solution rates in gypsum karst: Case study from the Western Ukraine”. In: *Environmental Geology* 48.3, pp. 307–319. ISSN: 0943-0105. DOI: \url{10.1007/s00254-005-1277-3}.

Klimchouk, A. B. et al. (1996). “Dissolution of gypsum from field observations”. In: *International Journal of Speleology* 25.3/4, pp. 37–48. ISSN: 0392-6672. DOI: \url{10.5038/1827-806X.25.3.3}.

Lakey, Barbara and Noel C. Krothe (1996). “Stable Isotopic Variation of Storm Discharge from a Perennial Karst Spring, Indiana”. In: *Water Resources Research* 32.3, pp. 721–731. ISSN: 00431397. DOI: \url{10.1029/95WR01951}.

Lee, Eung Seok and Noel C. Krothe (2001). “A four-component mixing model for water in a karst terrain in south-central Indiana, USA. Using solute concentration and stable isotopes as tracers”. In: *Chemical Geology* 179.1-4, pp. 129–143. DOI: \url{10.1016/S0009-2541(01)00319-9}.

— (2003). “Delineating the karstic flow system in the upper Lost River drainage basin, south central Indiana: Using sulphate and dSO4 as tracers”. In: *Applied Geochemistry* 18.1, pp. 145–153. ISSN: 08832927. DOI: \url{10.1016/S0883-2927(02)00067-7}.

Leibundgut, Christian, P. Maloszewski, and Christoph Külls (2009). *Tracers in Hydrology*. Chichester, UK: John Wiley & Sons, Ltd. ISBN: 9780470747148. DOI: \url{10.1002/9780470747148}.

Levenspiel, Octave (1999). “Chemical Reaction Engineering”. In: *Industrial & Engineering Chemistry Research* 38.11, pp. 4140–4143. ISSN: 0888-5885. DOI: \url{10.1021/ie990488g}.

Lindgren, G. A., G. Destouni, and A. V. Miller (2004). "Solute transport through the integrated groundwater-stream system of a catchment". In: *Water Resources Research* 40.3, n/a–n/a. ISSN: 00431397. DOI: \url{10.1029/2003WR002765}.

Lopez-Chicano, M. et al. (2001). "Factors which determine the hydrogeochemical behaviour of karstic springs. A case study from the Betic Cordilleras, Spain". In: *Applied Geochemistry* 16.9, pp. 1179–1192. ISSN: 08832927.

Maher, K. (2011). "The role of fluid residence time and topographic scales in determining chemical fluxes from landscapes". In: *Earth and Planetary Science Letters* 312.1-2, pp. 48–58. ISSN: 0012821X. DOI: \url{10.1016/j.epsl.2011.09.040}.

Maloszewski, P. and K. P. Seiler (2000). "Modelling of flow dynamics in layered groundwater systems—comparative evaluation of black box and numerical approaches." In: *Isotope Techniques in Water Resources Development and Management*. Ed. by IAEA. C&S Papers Series (CD-ROM). Vienna: IAEA.

Maloszewski, P. et al. (1992). "Isotope hydrological study of mean transit times in an Alpine Basin (Wimbachtal, Germany)". In: 140.1-4, pp. 343–360. DOI: \url{10.1016/0022-1694(92)90247-S}. URL: %5Curl%7Bhttps://www.researchgate.net/profile/Piotr_Maloszewski/publication/223488166_Isotope_hydrological_study_of_mean_transit_times_in_an_Alpine_Basin_Wimbachtal_Germany/links/54afff7b0cf28ebe92de3af5.pdf%7D.

Maloszewski, P. et al. (2002). "Identifying the flow systems in a karstic-fissured-porous aquifer, the Schneealpe, Austria, by modelling of environmental 18O and 3H isotopes". In: *Journal of Hydrology* 256.1-2, pp. 48–59. ISSN: 0022-1694. DOI: \url{10.1016/S0022-1694(01)00526-1}.

Marin, A., B. Andreo, and M. Mudarra (2010). "Importance of evaluating karst features in contamination vulnerability and groundwater protection assessment of carbonate aquifers. The case study of Alta Cadena (Southern Spain)". In: *Zeitschrift für Geomorphologie, Supplementary Issues* 54.2, pp. 179–194. ISSN: 18641687. DOI: \url{10.1127/0372-8854/2010/0054S2-0010}.

— (2015). "Vulnerability mapping and protection zoning of karst springs. Validation by multitracer tests". In: *The Science of the total environment* 532, pp. 435–446. ISSN: 0048-9697. DOI: \url{10.1016/j.scitotenv.2015.05.029}.

Martín-Algarra, A. (1987). *Evolucion geologica alpina del contacto entre las zonas internas y las externas de la Cordillera Betica (sector central y occidental): tesis doctoral*. Universitad, Depart. Estratigrafia y Paleontologia. URL: %5Curl%7Bhttps://books.google.de/books?id=zwWJoAEACAAJ%7D.

Martínez, M. M. et al. (2010). "Investigación del funcionamiento hidrogeológico del acuífero carbonatado drenado por el manantial de Villanueva del Rosario (Alta Cadena, Málaga) a partir de un ensayo de trazadores". In: *Geogaceta* 48, pp. 131–134.

Massey, Frank J. (1951). "The Kolmogorov-Smirnov Test for Goodness of Fit". In: *Journal of the American Statistical Association* 46.253, p. 68. ISSN: 01621459. DOI: \url{10.2307/2280095}.

McDonnell, J. J. et al. (2010). "How old is streamwater? Open questions in catchment transit time conceptualization, modelling and analysis". In: *Hydrological Processes* 24.12, pp. 1745–1754. ISSN: 08856087. DOI: \url{10.1002/hyp.7796}.

McGuire, Kevin J. and J. J. McDonnell (2006). "A review and evaluation of catchment transit time modeling". In: *Journal of Hydrology* 330.3, pp. 543–563. ISSN: 0022-1694. URL: %5Curl%7Bhttp://www.sciencedirect.com/science/article/pii/S0022169406002150%7D.

Mercado, A. and G. K. Billings (1975). "The kinetics of mineral dissolution in carbonate aquifers as a tool for hydrological investigations, I. Concentration-time relationships". In: *Journal of Hydrology* 24.3-4, pp. 303–331. ISSN: 0022-1694. DOI: \url{10.1016/0022-1694(75)90088-8}.

Milly, P. C. D., K. A. Dunne, and A. V. Vecchia (2005). "Global pattern of trends in streamflow and water availability in a changing climate". In: *Nature* 438.7066, pp. 347–350. ISSN: 0028-0836. DOI: \url{10.1038/nature04312}.

Morgenstern, U., M. Stewart, and R. Stenger (2010). "Dating of streamwater using tritium in a post nuclear bomb pulse world: Continuous variation of mean transit time with streamflow". In: *Hydrology and Earth System Sciences* 14.11, pp. 2289–2301. ISSN: 1607-7938. DOI: \url{10.5194/hess-14-2289-2010}.

Mudarra, M. and B. Andreo (2011). "Relative importance of the saturated and the unsaturated zones in the hydrogeological functioning of karst aquifers: The case of Alta Cadena (Southern Spain)". In: *Journal of Hydrology* 397.3-4, pp. 263–280. ISSN: 0022-1694. DOI: \url{10.1016/j.jhydrol.2010.12.005}.

Mudarra, M., B. Andreo, J. A. Barberá, et al. (2014). "Hydrochemical dynamics of TOC and NO3 − contents as natural tracers of infiltration in karst aquifers". In: *Environmental Earth Sciences* 71.2, pp. 507–523. ISSN: 1866-6299. DOI: \url{10.1007/s12665-013-2593-7}. URL: %5Curl%7Bhttp://link.springer.com/article/10.1007/s12665-013-2593-7/fulltext.html%7D.

Mudarra, M., B. Andreo, A. Marin, et al. (2014). "Combined use of natural and artificial tracers to determine the hydrogeological functioning of a karst aquifer: The Villanueva del Rosario system (Andalusia, southern Spain)". In: *Hydrogeology Journal* 22.5, pp. 1027–1039. ISSN: 1431-2174. DOI: \url{10.1007/s10040-014-1117-1}.

Nelder, J. A. and R. Mead (1965). "A Simplex Method for Function Minimization". In: *The Computer Journal* 7.4, pp. 308–313. ISSN: 0010-4620. DOI: \url{10.1093/comjnl/7.4.308}.

Niemi, Antti J. (1977). "Residence time distributions of variable flow processes". In: *The International Journal of Applied Radiation and Isotopes* 28.10-11, pp. 855–860. ISSN: 0020708X. DOI: \url{10.1016/0020-708X(77)90026-6}.

Oda, Tomoki, Yuko Asano, and Masakazu Suzuki (2009). "Transit time evaluation using a chloride concentration input step shift after forest cutting in a Japanese headwater catchment". In: *Hydrological Processes* 23.19, pp. 2705–2713. ISSN: 08856087. DOI: \url{10.1002/hyp.7361}.

ORNL DAAC (2008). *MODIS Collection 5 Global Subsetting and Visualization Tool: Accessed April 29, 2016. Subset obtained for MOD16A2 product at 36.8467N,4.4362W, time period: 2006-09-30 to 2009-10-16, and subset size: 201 x 201 km.* DOI: \url{10.3334/ORNLDAAC/1241}.

Ozyurt, N. Nur and C. Serdar Bayari (2005). "Steady- and unsteady-state lumped parameter modelling of tritium and chlorofluorocarbons transport: Hypothetical analyses and application to an alpine karst aquifer". In: *Hydrological Processes* 19.17, pp. 3269–3284. ISSN: 08856087. DOI: \url{10.1002/hyp.5969}.

Palmer, A. N. (1999). "Anisotropy in carbonate aquifers". In: *Karst modeling*. Ed. by A. N. Palmer, M. V. Palmer, and Ira D. Sasowsky. Vol. 5. Special publication. Charles Town, W. Va.: Karst Waters Institute, pp. 223–227. ISBN: 0964025841.

Perrin, J., P.-Y. Jeannin, and F. Cornaton (2007). "The role of tributary mixing in chemical variations at a karst spring, Milandre, Switzerland". In: *Journal of Hydrology* 332.1-2, pp. 158–173. ISSN: 0022-1694. DOI: \url{10.1016/j.jhydrol.2006.06.027}.

Peyre, Y. (1974). *Géologie d'Antequera et de sa region (Cordillères bétiques-Espagne): Description de la region d'Antequera et de ses contrees voisines (provinces de Malaga, Seville, Cordove et Grenade). I.* Travaux du Laboratoire de Géologie Méditerranéenne. Institut National Agronomique Paris-Grignon. URL: %5Curl%7Bhttps://books.google.de/books?id=tn2ZPAAACAAJ%7D.

Rinaldo, A. et al. (2011). "Catchment travel time distributions and water flow in soils". In: *Water Resources Research* 47.7, n/a–n/a. ISSN: 00431397. DOI: \url{10.1029/2011WR010478}.

Rinaldo, A. et al. (2015). "Storage selection functions: A coherent framework for quantifying how catchments store and release water and solutes". In: *Water Resources Research* 51.6, pp. 4840–4847. ISSN: 00431397. DOI: \url{10.1002/2015WR017273}.

Sauter, Martin (1997). "Differentiation of flow components in a karst aquifer using the d18O signature". In: *Tracer hydrology 97*. Ed. by Andrej Kranjc. Rotterdam and Brookfield, VT, USA: A.A. Balkema, pp. 435–441. ISBN: 9789054108757.

Sauter, Martin et al. (2006). "Modellierung der Hydraulik von Karstgrundwasserleitern – Eine Übersicht". In: *Grundwasser* 11.3, pp. 143–156. ISSN: 1430-483X. DOI: \url{10.1007/s00767-006-0140-0}.

Segura, C. et al. (2012). "Scaling relationships for event water contributions and transit times in small-forested catchments in Eastern Quebec". In: *Water Resources Research* 48.7, n/a–n/a. ISSN: 00431397. DOI: \url{10.1029/2012WR011890}.

Shuster, Evan T. and W. B. White (1971). "Seasonal fluctuations in the chemistry of lime-stone springs: A possible means for characterizing carbonate aquifers". In: *Journal of Hydrology* 14.2, pp. 93–128. ISSN: 0022-1694. DOI: \url{10.1016/0022-1694(71)90001-1}.

Sklash, Michael G. and Robert N. Farvolden (1979). "The Role of Groundwater in Storm Runoff". In: 43.1, pp. 45–65. DOI: \url{10.1016/0022-1694(79)90164-1}.

Spear, R. (1980). "Eutrophication in peel inlet—II. Identification of critical uncertainties via generalized sensitivity analysis". In: *Water Research* 14.1, pp. 43–49. ISSN: 00431354. DOI: \url{10.1016/0043-1354(80)90040-8}.

Stevanović, Zoran, N. Goldscheider, and Zhao Chen (2016). "WOKAM – The world karst aquifer mapping project, examples from South East Europe, Near and Middle East and Eastern Africa". In: *Karst without Boundaries*. Ed. by Zoran Stevanović, Neven Krešić, and Neno Kukurić. Vol. v.23. IAH - Selected Papers on Hydrogeology. London: CRC Press, pp. 39–51. ISBN: 978-1-138-02968-2. DOI: \url{10.1201/b21380-5}.

Stumpp, Christine, Willibald Stichler, and P. Maloszewski (2009). "Application of the environmental isotope d18O to study water flow in unsaturated soils planted with different crops: Case study of a weighable lysimeter from the research field in Neuherberg, Germany". In: *Journal of Hydrology* 368.1-4, pp. 68–78. ISSN: 0022-1694. DOI: \url{10.1016/j.jhydrol.2009.01.027}.

Szilagyi, Jozsef, Marc B. Parlange, and John D. Albertson (1998). "Recession flow analysis for aquifer parameter determination". In: *Water Resources Research* 34.7, pp. 1851–1857. ISSN: 00431397. DOI: \url{10.1029/98WR01009}.

Tallaksen, L. M. (1995). "A review of baseflow recession analysis". In: *Journal of Hydrology* 165.1-4, pp. 349–370. ISSN: 0022-1694. DOI: \url{10.1016/0022-1694(94)02540-R}.

Teutsch, G. (1988). *Grundwassermodelle im Karst: praktische Ansätze am Beispiel zweier Einzugsgebiete im tiefen und seichten Malmkarst der Schwäb. Alb*. URL: %5Curl%7Bhttps://books.google.de/books?id=N0n9ngEACAAJ%7D.

Thornthwaite, C. W. (1948). "An Approach toward a Rational Classification of Climate". In: *Geographical Review* 38.1, p. 55. ISSN: 00167428. DOI: \url{10.2307/210739}.

van der Velde, Y. et al. (2010). "Nitrate response of a lowland catchment: On the relation between stream concentration and travel time distribution dynamics". In: *Water Resources Research* 46.11. ISSN: 1944-7973. DOI: \url{10.1029/2010WR009105}. URL: %5Curl%7Bhttp://onlinelibrary.wiley.com/doi/10.1029/2010WR009105/full%7D.

van der Velde, Y. et al. (2012). "Quantifying catchment-scale mixing and its effect on time-varying travel time distributions". In: *Water Resources Research* 48.6. ISSN: 00431397. DOI: \url{10.1029/2011WR011310}.

Weiler, M. et al. (2003). "How does rainfall become runoff? A combined tracer and runoff transfer function approach". In: *Water Resources Research* 39.11, n/a–n/a. ISSN: 00431397. DOI: \url{10.1029/2003WR002331}.

White, W. B. (2002). "Karst hydrology: Recent developments and open questions". In: *Engineering Geology* 65.2-3, pp. 85–105. ISSN: 00137952. DOI: \url{10.1016/S0013-7952(01)00116-8}.

Williams, P.W. (2008). "The role of the epikarst in karst and cave hydrogeology: A review". In: *International Journal of Speleology* 37.1, pp. 1–10. ISSN: 0392-6672. DOI: \url{10.5038/1827-806X.37.1.1}.

Worthington, S. R. H. and D. C. Ford (1995). "High sulfate concentrations in limestone springs: An important factor in conduit initiation?" In: *Environmental Geology* 25.1, pp. 9–15. ISSN: 0943-0105. DOI: \url{10.1007/BF01061825}.

Wright, M. H. (1996). "Direct Search Methods: Once Scorned, Now Respectable". In: *Numerical Analysis 1995: Proceedings of the 1995 Dundee Biennial Conference in Numerical Analysis*. Ed. by D.F. Griffiths and G.A. Watson. Harlow, UK: Addison Wesley Longman, pp. 191–208.

Zwahlen, F. (2004). *Cost action 620: Vulnerability and risk mapping for the protection of carbonate (karst) aquifers : final report*. Luxembourg: Office for Official Publications of the European Communities. ISBN: 9789289464161.

Appendix

Additional Figures

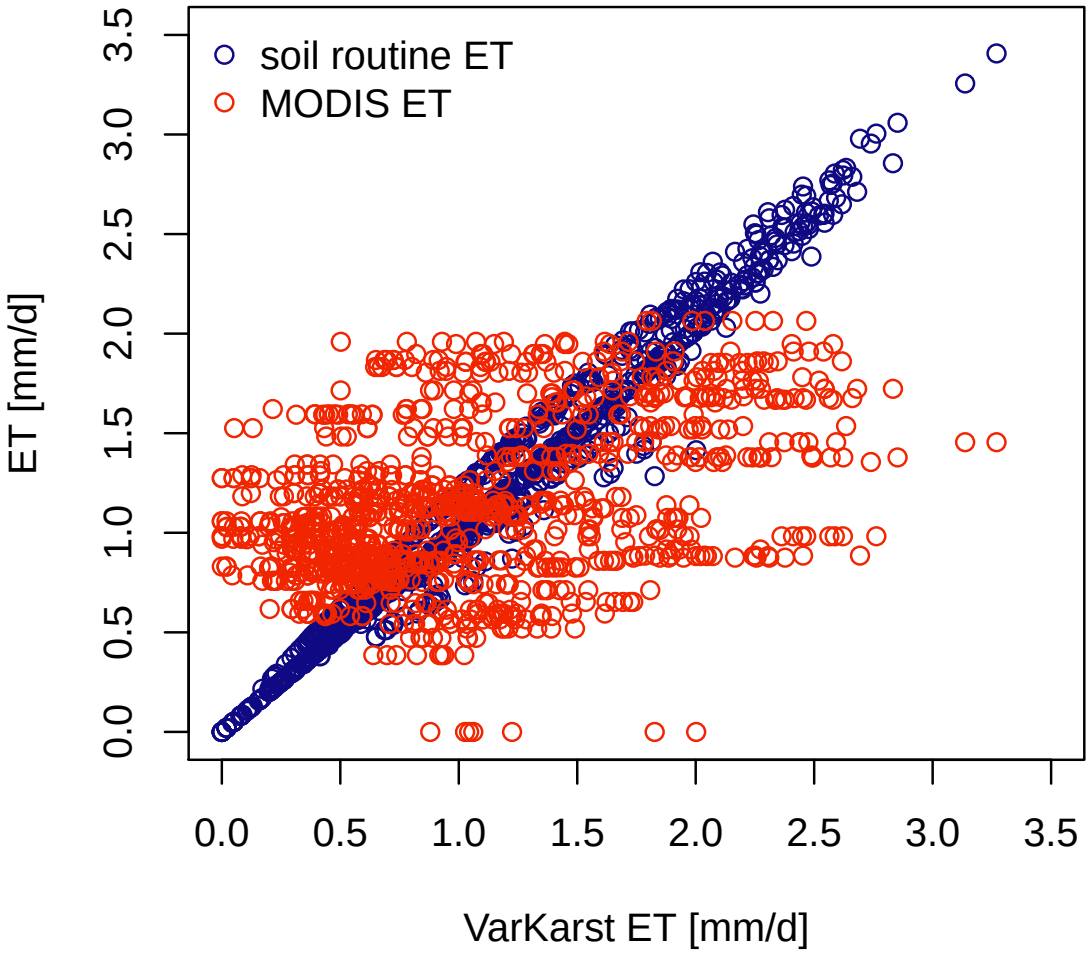

Figure 6.1: ET of the benchmark model VarKarst versus 1. ET from MODIS data (ORNL DAAC, 2008), 2. ET calculated through soil routine (Kirn et al., 2016).

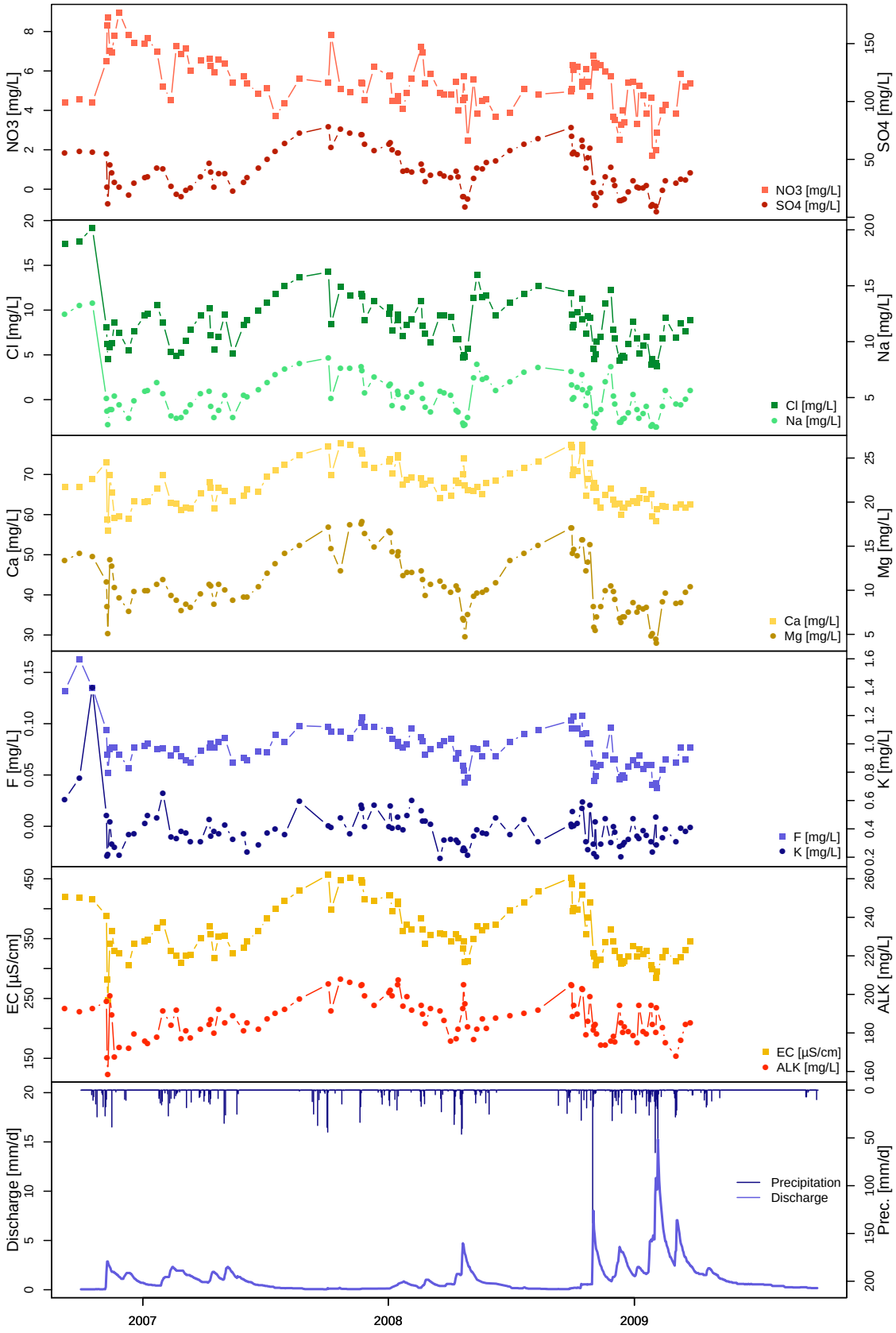

Figure 6.2: Time series of all available solutes and hydrochemical parameters measured in the spring discharge.

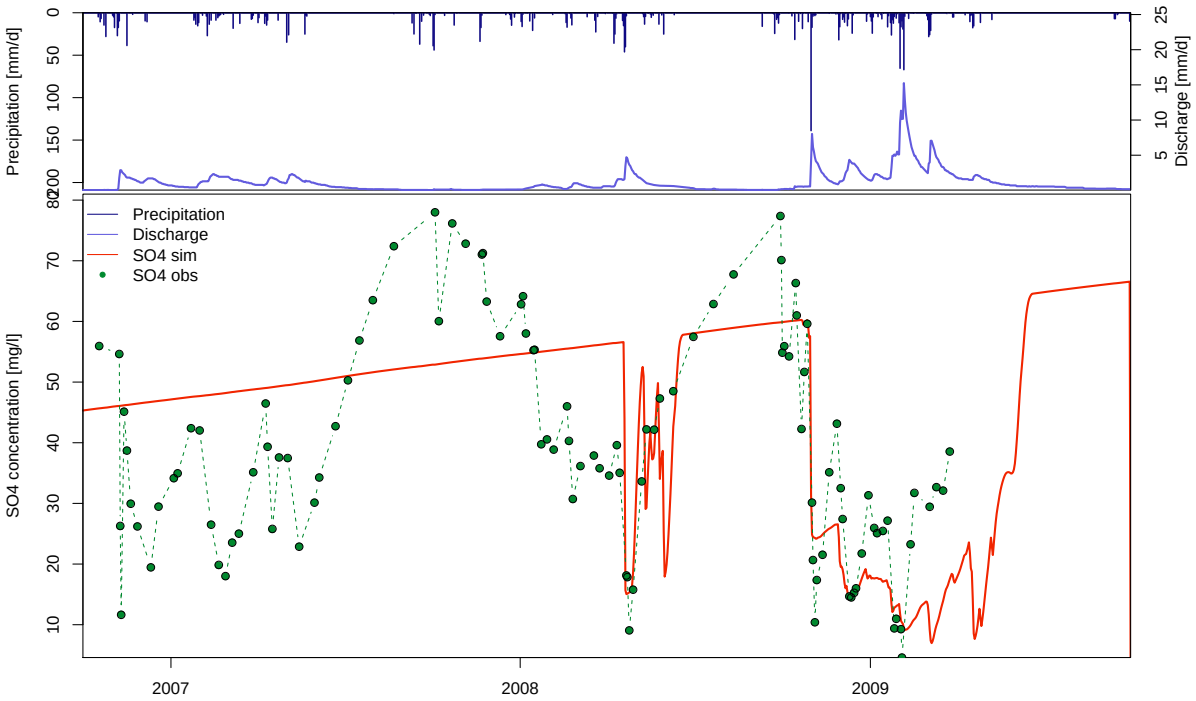

Figure 6.3: Time series of predicted sulfate concentration (SO4 sim) and observed sulfate concentration (SO4 obs) in the discharge calculated with a time-invariant gamma function. Precipitation input and spring hydrograph time series for comparison.

Python code: rSAS, HSY and GLUE

```
# -*- coding: utf-8 -*-
"""
Created on Tue Jun 28 10:38:16 2016

@author: Lina Stein
"""
#~~~~~~~~~~~~~~~~~~~~~~~~~~~~~~~~~~~~~~~~~~~~~~~~~~~~~~~~~~~~~~~~~~~~~~~~~~~~~~~
#~~~~~~~~~~~~~~~~~~~~~~~~~~~~~~~~~~~~~~~~~~~~~~~~~~~~~~~~~~~~~~~~~~~~~~~~~~~~~~~
```

```
#Calculate solute transport by applying age-ranked StorAge Selection functions
#Concept explained in:
#Harman, C. J. (2015). Time-variable transit time distributions and transport:
#Theory and application to storage-dependent transport of chloride in a
#watershed.
#Water Resources Research, 51(1), 1-30.
#~~~~~~~~~~~~~~~~~~~~~~~~~~~~~~~~~~~~~~~~~~~~~~~~~~~~~~~~~~~~~~~~~~~~~~~~~~~~
#~~~~~~~~~~~~~~~~~~~~~~~~~~~~~~~~~~~~~~~~~~~~~~~~~~~~~~~~~~~~~~~~~~~~~~~~~~~~
import pandas as pd
import numpy as np
import matplotlib.pylab as plt
import rsas
import os
os.chdir('C:\Users\Lina\Studium\Masterarbeit\Data')
# ============================================================================
# Set up inputs
# ============================================================================
input_filename='AET_HCmat_SO4.csv'
df_data=pd.read_csv(input_filename, parse_dates=True, index_col=0)
return_obs=True
#redefine and adjust variables
N = len(df_data)
C_in = df_data['C_J'].values    #input concentration
C_in=np.array(C_in)
Q = df_data['Q1'].values        #discharge
P = df_data['J'].values         #precipitation
C_out = df_data['C_Q1'].values  #output concentration
S = df_data['S'].values         #storage
ET = df_data['ET'].values       #evapotranspiration
dS = S-np.mean(S)
ET_S = 1000  #ST_max for evapoconcentration rSAS
C_old_rsas = [0.]
C_old_transport = [0.]
## Unknown total storage
```

```
MS_init = np.zeros((N + 1, 1))
S_large = 10000
ST_init = np.ones(N+1) * S_large
ST_init[0] = 0.
#set up inputs (one flux discharge, one flux ET)
flux = np.ones((N, 2))
flux[:,0]=Q
flux[:,1]=ET
alpha = np.ones((2,1))
alpha[0,0] = 1.
alpha[1,0] = 0.

#%%
# ========================================================================
# Define rSAS for optimization run
# ========================================================================

def run(params):
    C_back1, k1_1, C_eq_1, Logalpha, lambd, dS_crit = params
    CS_initf = np.ones((N,1)) * C_back1
    k1f = np.ones((N,1)) * k1_1
    C_eqf = np.ones((N,1)) * C_eq_1
    #rSAS
    Q_rSAS_fun_type = 'gamma'
    ST_min = np.ones(N) * 0.
    ST_max = np.ones(N) * np.inf
    d_alpha = np.ones(N) * np.exp(Logalpha)
    d_beta = np.maximum(0.01, (lambd/d_alpha)*(dS-dS_crit) )
    Q_rSAS_fun_parameters = np.c_[ST_min, ST_max, d_beta, d_alpha] #scale, shape
    rSAS_fun_Q = rsas.create_function(Q_rSAS_fun_type, Q_rSAS_fun_parameters)
    # - ET
    ET_rSAS_fun_type = 'uniform'
    ET_rSAS_fun_parameters = np.c_[np.zeros(N), np.ones(N) * ET_S ]
    rSAS_fun_ET = rsas.create_function(ET_rSAS_fun_type, ET_rSAS_fun_parameters)
```

```
    # Run it
    outputs = rsas.solve(P, flux, [rSAS_fun_Q, rSAS_fun_ET], ST_init=ST_init,
                         mode='RK4', dt = 1., n_substeps=1,verbose=False,
                         debug=False, C_J=C_in, C_old=C_old_rsas, CS_init=CS_initf,
                         alpha=alpha, k1=k1f, C_eq=C_eqf)

    return outputs

def err(params):
    outputs = run(params)
    C_Q = outputs['C_Q'][:,0,0]
    #mask to filter NA
    isobs = np.isfinite(C_out)
    #calculate KGE
    r = np.corrcoef(C_out[isobs], C_Q[isobs])[0,1]
    KGE_alpha = (np.std(C_Q[isobs])/np.std(C_out[isobs]))
    KGE_beta = (np.mean(C_Q[isobs])/np.mean(C_out[isobs]))
    err = np.sqrt((((r-1)**2)+((KGE_alpha-1)**2)+((KGE_beta-1)**2)))

    print params, err
    return err
#%%
# ============================================================================
# Find optimum parameter set
# ============================================================================
#for SO4
params0 = [50., 0.001, 90., -1.6, -1.5, 200.]
# run the optimzer
from scipy.optimize import fmin
params_opt = fmin(err, params0)
C_back1, k1_1, C_eq_1, Logalpha, lambd, dS_crit  = params_opt
print "Optimum parameter set = ", params_opt
# extract the outputs
```

```
outputs = run(params_opt)
C_Q = outputs['C_Q'][:,0,0]
ST = outputs['ST']
PQ1m = outputs['PQ'][:,:,0]
#%%
# ============================================================================
# Plot results optimized parameters
# ============================================================================
dates = df_data['datetime']
datetime = pd.to_datetime(dates, format="%Y-%m-%d")
fig = plt.figure(figsize = (6.5, 10))
#plot Q
ax = fig.add_subplot(411)
ax.plot(datetime, Q, label='Discharge')
plt.legend(loc=1, frameon=True, fontsize=8)
#plot P
ax = fig.add_subplot(412)
ax.plot(datetime, P, label='Precipitation')
plt.legend(loc=1, frameon=True, fontsize=8)
#plot C_in
ax = fig.add_subplot(413)
ax.plot(datetime, C_in, label='Input Concentration [mg/l]')
plt.legend(loc=1, frameon=True, fontsize=8)
#plot C_out and simulated
ax = fig.add_subplot(414) #414
ax.plot(datetime, df_data['C_Q1'], 'r.',
        label='Output Concentration observed [mg/l]', zorder=1)
ax.plot(datetime, C_Q, 'b-', label='Output Concentration simulated [mg/l]')
plt.ylim((0, 90))
plt.legend(loc=1, frameon=True, fontsize=8)
plt.tight_layout()
#%%
# ============================================================================
# Plot the rSAS function
```

```
# ========================================================================
STx = np.linspace(0,S.max(),500) #S.max()+S_dead
Omega = np.r_[[rSAS_fun_Q.cdf_i(STx,i) for i in range(N)]].T
import matplotlib.cm as cm
#graphical parameters
norm = cm.colors.Normalize(vmin=np.min(S),vmax=np.max(S))
c_m = cm.jet
s_m = cm.ScalarMappable(cmap=c_m, norm=norm)
s_m.set_array([])

fig = plt.figure(13)
plt.clf()
for i in range(N):
    plt.plot(STx, Omega[:,i], lw=1, color=cm.jet((S[i]-S.min())/S.ptp()))
plt.ylim((0,1))
plt.colorbar(s_m)
plt.ylabel('$\Omega_Q(T)$')
plt.xlabel('age-ranked storage $S_T$')
plt.title('Cumulative rSAS function magnesium')
plt.text(360, -0.08, 'Storage [mm]')
#%%
# ========================================================================
# Plot the actual transit time distribution
# ========================================================================
fig = plt.figure(1)
plt.clf()
plt.plot(PQ1m, lw=1)
plt.ylim((0,1))
plt.ylabel('$P_Q(T)$')
plt.xlabel('age $T$')
plt.title('Cumulative transit time distribution')
#%%
# ========================================================================
# Define rSAS for GLUE
```

```
# ========================================================================
def run(params):
    C_back1, k1_1, C_eq_1, Logalpha, lambd, dS_crit = params
    CS_initf = np.ones((N,1)) * C_back1
    k1f = np.ones((N,1)) * k1_1
    C_eqf = np.ones((N,1)) * C_eq_1
    #rsas
    Q_rSAS_fun_type = 'gamma'
    ST_min = np.ones(N) * 0.
    ST_max = np.ones(N) * np.inf
    d_alpha = np.ones(N) * np.exp(Logalpha)
    d_beta = np.maximum(0.01, (lambd/d_alpha)*(dS-dS_crit) )
    Q_rSAS_fun_parameters = np.c_[ST_min, ST_max, d_beta, d_alpha] #scale, shape
    rSAS_fun_Q = rsas.create_function(Q_rSAS_fun_type, Q_rSAS_fun_parameters)
    # - ET
    ET_rSAS_fun_type = 'uniform'
    ET_rSAS_fun_parameters = np.c_[np.zeros(N), np.ones(N) * ET_S ]
    rSAS_fun_ET = rsas.create_function(ET_rSAS_fun_type, ET_rSAS_fun_parameters)

    # Run it
    outputs = rsas.solve(P, flux, [rSAS_fun_Q, rSAS_fun_ET], ST_init=ST_init,
                     mode='RK4', dt = 1., n_substeps=1,verbose=False,
                     debug=False, C_J=C_in, C_old=C_old_rsas, CS_init=CS_initf,
                     alpha=alpha, k1=k1f, C_eq=C_eqf)
    C_Q = outputs['C_Q'][:,0,0]
    isobs = np.isfinite(C_out)
    r = np.corrcoef(C_out[isobs], C_Q[isobs])[0,1]
    KGE_alpha = (np.std(C_Q[isobs])/np.std(C_out[isobs]))
    KGE_beta = (np.mean(C_Q[isobs])/np.mean(C_out[isobs]))
    err = 1-np.sqrt((((r-1)**2)+((KGE_alpha-1)**2)+((KGE_beta-1)**2)))

    C_Q = outputs['C_Q'][:,0,0]

    return err, C_Q
```

```
#%%
# ============================================================================
# GLUE
# ============================================================================
GlueRuns = 30000
Nparams = 6
#Define limits
#SO4 (+-75 %, except alpha and k1 )
upLim = [68. ,0.01 , 338. ,0. ,-0.34, 469. ]* np.ones(Nparams)
loLim = [10. ,0.0003 , 48. ,-2. ,-2.4, 67. ]* np.ones(Nparams)
##Cl (+-75 %, except alpha and k1 )
#upLim = [49. ,0.01 , 140. ,0. ,-0.28, 450. ]* np.ones(Nparams)
#loLim = [7. ,0.0002 , 20. ,-2. ,-1.95, 64. ]* np.ones(Nparams)
#Empty matrix for parameter storage
ParMat = np.zeros((GlueRuns,Nparams))
#randomly chooses parameter inside limits
for i in range(0, Nparams):
    ParMat[:,i] = np.random.uniform(loLim[i], upLim[i],(GlueRuns,) )

EffMat = np.zeros(GlueRuns) #store efficiencies
CQMat = np.zeros((GlueRuns,N)) #store output concentrations

for i in range(0, GlueRuns):
    err, CQ_sim = run(ParMat[i,])
    EffMat[i] = err
    CQMat[i] = CQ_sim
    print(i)

#save arrays for HSY analysis in R
np.savetxt('C:\Users\Lina\Studium\Masterarbeit\
                    Data\GLUE\EffMat30000_11_SO4.txt', EffMat)
np.savetxt('C:\Users\Lina\Studium\Masterarbeit\
                    Data\GLUE\ParMat30000_11_SO4.txt', ParMat)
np.savetxt('C:\Users\Lina\Studium\Masterarbeit\
```

```
                    GLUEdata\CQMat30000_11_SO4.txt', CQMat)
CQMatPlot = CQMat
EffMatPlot = EffMat
EffMatPlot = np.reshape(EffMatPlot, (GlueRuns,1))
ParMatPlot = ParMat
#combine arrays
fullMat = np.concatenate((EffMatPlot,ParMatPlot, CQMat), axis=1)
fullMat_sort = fullMat[np.argsort(fullMat[:, 0])]
#split into behavioural and non-behavioural runs
behavMat = fullMat_sort[-500:,:][::-1]
nonbehavMat = fullMat_sort[range(0,GlueRuns-500),:][::-1]
#calculate 95% confidence interval
perc_b_97_5 = np.apply_along_axis(lambda x: np.percentile(x,97.5), 0,
                                  behavMat[:,range(7,N+7)])
perc_b_2_5 = np.apply_along_axis(lambda x: np.percentile(x,2.5), 0,
                                 behavMat[:,range(7,N+7)])
perc_b_50 = np.apply_along_axis(lambda x: np.percentile(x,50), 0,
                                behavMat[:,range(7,N+7)])

#save percentiles for plotting in R
perc_mat = np.stack((perc_b_97_5,perc_b_2_5, perc_b_50,
                     behavMat[0, range(7,N+7)], df_data['C_Q1'] ), axis=-1)
```

Acronyms

AET	actual evapotranspiration
ALK	gran alkalinity
α	alpha
ASL	above sea level
bTTD	backward transit time distribution
Ca^{2+}	calcium
C_{back}	background concentration
C_{eq}	equilibrium concentration
C_{in}	input concentration
Cl^-	chloride
EC	electrical conductivity
eCDF	empirical cumulative distribution function
ED	Euclidian distance
F^-	fluoride
fTTD	forward transit time distribution
GLUE	Generalized likelihood uncertainty estimation
HSY	Hornberge-Spear-Young
K^+	potassium
k1	reaction rate
KGE	Kling-Gupta efficiency
KS test	Kolmogorov–Smirnov test
λ	lambda
Mg^{2+}	magnesium

Na^+	sodium
NO_3^-	nitrate
$logP_{CO2}$	log. partial pressure of carbon dioxide
PDF	probability density function
PET	potential evapotranspiration
RTD	residence time distribution
SAS	StorAge Selection
dS_{crit}	critical storage
$SI_{calcite}$	saturation index with respect to calcite
SO_4^{2-}	sulfate
T	water age, $T = t - t_i$
t	time or exit time
t_i	input time
T_W	water temperature
TTD	transit time distribution

Ehrenwörtliche Erklärung

Hiermit erkläre ich, dass die Arbeit selbständig und nur unter Verwendung der angegebenen Hilfsmittel angefertigt wurde.

Ort, Datum *Unterschrift*